Title

Mechanisms underlying divergent relationships between Ca2+ and YAP/TAZ signalling.

Journal

The Journal of Physiology, 601(3)

Authors

Khalilimeybodi, A

Fraley, Stephanie

Rangamani, Padmini

et al.

Publication Date

2023-02-01

DOI

10.1113/JP283966

Peer reviewed

Published in final edited form as:
J Physiol. 2023 February ; 601(3): 483–515. doi:10.1113/JP283966.

Mechanisms underlying divergent relationships between Ca^{2+} and YAP/TAZ signaling

A. Khalilimeybodi[1], **S.I. Fraley**[2,*], **P. Rangamani**[1,*]

[1]Department of Mechanical and Aerospace Engineering, Jacobs School of Engineering, University of California San Diego, La Jolla CA 92093.

[2]Department of Bioengineering, Jacobs School of Engineering, University of California San Diego, La Jolla CA 92093.

Abstract

Yes-associated protein (YAP) and its homolog TAZ are transducers of several biochemical and biomechanical signals, integrating multiplexed inputs from the microenvironment into higher-level cellular functions such as proliferation, differentiation, and migration. Emerging evidence suggests that Ca^{2+} is a key second messenger that connects microenvironmental input signals and YAP/TAZ regulation. However, studies that directly modulate Ca^{2+} have reported contradictory YAP/TAZ responses: In some studies, a reduction in Ca^{2+} influx increases the activity of YAP/TAZ, while in others, an increase in Ca^{2+} influx activates YAP/TAZ. Importantly, Ca^{2+} and YAP/TAZ exhibit distinct spatiotemporal dynamics, making it difficult to unravel their connections from a purely experimental approach. In this study, we developed a network model of Ca^{2+}-mediated YAP/TAZ signaling to investigate how temporal dynamics and crosstalk of signaling pathways interacting with Ca^{2+} can alter YAP/TAZ response, as observed in experiments. By including six signaling modules (e.g., GPCR, IP3-Ca^{2+}, Kinases, RhoA, F-actin, and Hippo-YAP/TAZ) that interact with Ca^{2+}, we investigated both transient and steady-state cell response to Angiotensin II and thapsigargin stimuli. The model predicts that stimuli, Ca^{2+} transients, and frequency-dependent relationships between Ca^{2+} and YAP/TAZ are primarily mediated by cPKC, DAG, CaMKII, and F-actin. Simulation results illustrate the role of Ca^{2+} dynamics and CaMKII bistable response in switching the direction of changes in Ca^{2+}-induced YAP/TAZ activity. Frequency-dependent YAP/TAZ response revealed the competition between upstream regulators of LATS1/2, leading to the YAP/TAZ non-monotonic response to periodic GPCR stimulation. This study provides new insights into underlying mechanisms responsible for the controversial Ca^{2+}-YAP/TAZ relationship observed in experiments.

Keywords

YAP/TAZ; Calcium signaling; Network modeling; PKC isoforms; Hippo pathway

[*]To whom correspondence must be addressed: sifraley@ucsd.edu and prangamani@ucsd.edu.

Conflict of interests
All authors declare that they have no conflicts of interest.

1 Introduction

In any given cell, numerous external biochemical and biomechanical cues with different dynamics act together to control the cell's functions and phenotypic changes (Miller & Davidson, 2013; Artemenko et al., 2016). The intracellular interaction between these stimuli is orchestrated through a myriad signaling pathways enabling the cell to respond to various inputs proportional to their dynamics (Lauffenburger, 2000; Azeloglu & Iyengar, 2015). Yes-associated protein (YAP) and its homolog, transcriptional coactivator with PDZ-binding motif (TAZ), have recently attracted researchers' attention as key targets for integrating biochemical and biomechanical signals (Guo & Zhao, 2013; Totaro et al., 2018). The role of YAP/TAZ in regulating many cellular functions such as proliferation, differentiation, apoptosis, migration, and homeostasis has been demonstrated by the previous studies (Dupont et al., 2011; Barra Avila et al., 2021). The underlying mechanisms of YAP/TAZ activation have been studied in many fields, especially developmental and cancer biology (Pocaterra et al., 2020). Activation of YAP/TAZ is common in many human cancer tumors, where YAP/TAZ activity is crucial for cancer incidence and progression. Therefore, YAP/TAZ and its upstream signaling could be promising drug targets for metastatic tumors (Zanconato et al., 2016). YAP/TAZ responds to different cues by shuttling between the cytoplasm (inactive state) and nucleus (active state) to activate its cofactors, such as TEA domain transcription factors (TEADs), and thereby regulate the cell functions (Moroishi et al., 2015; Totaro et al., 2018). Although the upstream pathways of YAP/TAZ activation have been explored (Cai et al., 2021; Barra Avila et al., 2021), the YAP/TAZ response when multiple upstream signals exhibiting different dynamics act together like in GPCR signaling is not straightforward (Yu et al., 2012). This complexity and, in some cases, uncertainty in YAP/TAZ response (e.g., Ca^{2+}-induced YAP/TAZ) prevents us from understanding the dynamics of cellular functions controlled by YAP/TAZ activity (Hong & Guan, 2012; Shin & Nguyen, 2016; Ma et al., 2019).

The Hippo core cascade and the Rho family of GTPases (RhoA) pathways are primary transducers of several biochemical and biomechanical signals to YAP/TAZ (Low et al., 2014). The Hippo core cascade, including Mammalian STE20-like protein kinase 1/2 (MST1/2) and large tumor suppressors 1 and 2 (LATS1/2), is among the first discovered regulators of YAP/TAZ (Piccolo et al., 2014), extensively studied in cancer research for its tumor suppressor function mainly through YAP/TAZ inhibition (Hao et al., 2008; Furth et al., 2018). Numerous intrinsic and extrinsic signals can activate the Hippo pathway, including extracellular matrix (ECM) stiffness, cell polarity, cell-cell interaction, cellular energy status, and hormonal signals through GPCRs (Meng et al., 2016; Bae & Luo, 2018). RhoA pathway is an established and well-characterized master regulator of actin remodeling and cytoskeletal dynamics that can activate YAP/TAZ (Spiering & Hodgson, 2011; Jang et al., 2020). RhoA can be activated by mechanical stresses such as cell stretch, elevated ECM stiffness, and endogenous tension (Lessey et al., 2012; Haws et al., 2016). While the contribution of the Hippo and RhoA pathways to YAP/TAZ regulation is demonstrated by many studies (Dupont et al., 2011; Kodaka & Hata, 2015), there is a gap in the early upstream regulators of YAP/TAZ activity and their dynamics, especially by G-protein coupled receptors (GPCRs) agonists (Yu et al., 2012). Ca^{2+} has recently been

identified as a potential second messenger that closely connects the regulators of YAP/TAZ (Wei & Li, 2021) and actively participates in the YAP/TAZ regulation by mechanical and biochemical stimuli (Liu et al., 2019; Rodriguez et al., 2019; Wang et al., 2020). However, the contribution of Ca^{2+} to divergent responses of YAP/TAZ that have been observed in various experimental settings is not completely understood (Wei & Li, 2021). In this work, we aim to close this gap using computational modeling.

Ca^{2+} signaling can both inhibit and promote YAP/TAZ activity in various contexts, e.g., cell type, stimuli, and experiment conditions (Wei & Li, 2021) (Fig. 1A). In support of the inhibitory action of Ca^{2+} on YAP/TAZ, a study showed that Amlodipine, an L-type Ca^{2+} channel blocker, enhanced store-operated Ca^{2+} entry (SOCE) and led to elevated cytosolic Ca^{2+} level and the subsequent activation of the Hippo pathway resulting in the inhibition of YAP/TAZ in LN-229 cells (Liu et al., 2019). Also, the knockout of two-pore channel 2 (TPC2) increased YAP/TAZ activity in CHL1 and MeWo metastatic melanoma cells by reducing Ca^{2+} influx (D'Amore et al., 2020). On the other hand, some studies have demonstrated the activation of YAP/TAZ by Ca^{2+}. For example, activation of the Piezo1 receptor by mechanical stimuli (such as ECM stiffness) increases Ca^{2+} influx through Piezo1 and results in YAP nuclear localization or activation in human neural stem/progenitor cells (hNSPCs) (Pathak et al., 2014). Another study found that cholesterol can activate TAZ in AML12 cells by promoting the IP_3R activity, leading to higher cytosolic Ca^{2+} (Wang et al., 2020). Part of this bidirectional response can be associated with the cell type-dependent response of YAP/TAZ to protein kinase C (PKC) isoforms (Gong et al., 2015). Although all PKC isoforms have been demonstrated as regulators of YAP/TAZ activity in cells, their mechanisms of action are quite different. For example, while cPKCs promote YAP dephosphorylation (activation), nPKCs promote YAP phosphorylation, both through Hippo pathway regulation (Gong et al., 2015). Moreover, the Ca^{2+}-induced F-actin remodeling and subsequent elevation of cPKC (PKCβ) activity could lead to Hippo pathway activation and YAP/TAZ inhibition (Wei & Li, 2021). On the other hand, aPKC overexpression could increase YAP/TAZ activity by inhibiting MST1/2 from phosphorylating LATS1/2 (Archibald et al., 2015). However, to our knowledge, no experimental or computational studies have investigated underlying mechanisms that drive the bidirectional changes in Ca^{2+}-induced YAP/TAZ activity. Here, we investigate the contribution of PKC isoforms to Ca^{2+}-induced YAP/TAZ activity.

Our overarching hypothesis is that the different dynamics of signaling modules and species that link cell cues to Ca^{2+} and YAP/TAZ, as well as cell type-dependent differences in the Ca^{2+} transients, could modify Ca^{2+}-YAP/TAZ interaction. We developed a dynamical systems model of Ca^{2+}-mediated YAP/TAZ signaling based on prior knowledge to examine our hypothesis and calibrated our model with published experimental data. To investigate the effect of distinct biochemical signals on intracellular Ca^{2+} transients and subsequent YAP/TAZ regulation, we modeled Ca^{2+} dynamics induced by a Gq receptor agonist, Angiotensin II, and compared this to a SERCA inhibitor, thapsigargin. In the model, signal transduction from receptors to YAP/TAZ includes multiple biological processes such as membrane transduction, biochemical reactions, cytoskeletal changes, and nuclear translocation that take place on a seconds-to-day timescale (Fig. 1B). The inherent difference in the dynamics of these processes enables the cells to produce long-term

phenotypic changes in response to fast and transient input signals (Kholodenko, 2006). Given the importance of YAP/TAZ in cancer biology, most available experimental data on YAP/TAZ signaling, including data addressing its interaction with Ca^{2+} signaling, are from cancer cell lines that are generally categorized as non-excitable cells. Thus, building a model representing general non-excitable cells facilitates exploring the impact of different cell contexts, including cell stimuli (type and frequency) and cell type (Ca^{2+} transient), on YAP/TAZ activity through varying model parameters.

In summary, we mechanistically investigate the Ca^{2+}-YAP/TAZ relationship and predict potential mechanisms that modify this relationship in the cell. We identified the main signaling species in Ca^{2+}-mediated YAP/TAZ response and predicted how calcium/calmodulin-dependent protein kinase II (CaMKII) bistability could govern the switching from Ca^{2+}-induced YAP/TAZ inhibition to activation and vice versa. By exploring the influence of Gq receptor stimulation frequency on YAP/TAZ activity, we predict a YAP/TAZ non-monotonic response to periodic GPCR stimulation mainly mediated by LATS1/2. Finally, the model can explain the diverse Ca^{2+}-YAP/TAZ relationships reported in experimental studies.

2 Methods

2.1 Model development

Here, we describe the main features of our deterministic signaling model that investigates the crosstalk between intracellular Ca^{2+} dynamics and the activation of YAP/TAZ. We developed a compartmental ordinary differential equations (ODEs) model with seven (7) compartments to describe the dynamics of Ca^{2+}-mediated YAP/TAZ activation. The seven compartments include four (4) volumetric compartments, including the extracellular matrix (ECM), cytosol (C), endoplasmic reticulum (ER), and nucleus (N), and three membranes, including plasma membrane (PM), ER membrane (ERM), and nuclear membrane (NM). The concentrations of species in volumetric compartments are given in μM. Membrane-associated species are represented by their density in the membrane (molecules/μm^2). The model includes 74 signaling species linking biochemical and biomechanical inputs received by receptors on the plasma membrane to YAP/TAZ through 66 reactions. In the model, we assumed that all species are well mixed within their compartment and interactions between compartments are represented through fluxes.

The list of model species, including their best guess initial values obtained from previous studies or assumed in this study, is presented in Table 1. We simulated cell response from a steady state resting condition achieved by simulating the model without any inputs for a long time (100,000 s). These concentrations are provided in Table 1 and used as initial conditions for the main simulations in the result section. The reactions have been modeled mainly by mass action, Michaelis–Menten, and Hill kinetics originating from previously published models (Kowalewski et al., 2006; Maurya & Subramaniam, 2007; Dupont et al., 2016; Scott et al., 2021). Tables 2, 3, and 4 describe the reactions used in the model, including the reaction rate formula and kinetic parameters directly obtained from previous studies or estimated from experimental data. We focused on a generic mammalian cell rather than a specific cell type in our model. Therefore, we used previously published computational

models and empirical data from various non-excitable cell types to develop our model and estimate the parameters.

2.2 Main signaling modules

To understand the dynamics of Ca^{2+}-mediated pathways and evaluate their contribution to YAP/TAZ activity, we developed a model involving main pathways that connects biochemical and biomechanical signals to YAP/TAZ through Ca^{2+}. The model was constructed in a modular fashion to incorporate different pathways involved in Ca^{2+}-mediated YAP/TAZ signaling and is illustrated in Fig.1B. The model involves six (6) closely interacting modules (i.e., GPCR, IP_3-Ca^{2+}, Kinases, RhoA, F-actin, and Hippo-YAP/TAZ) with Ca^{2+} as the primary second messenger. As shown in Fig. 1B, experiments have established that the response times and dynamics of the modules cover a relatively broad range of timescales and behaviors due to the diversity in cell types, input signals, and signaling species in each module. Fast modules like GPCR respond to the input signals (e.g., Ang II) and reach a steady state in the order of seconds compared to slow modules like Hippo/YAP/TAZ, which could take several hours to reach their steady state. Intermediate modules (e.g., kinases module) respond to their inputs in the order of minutes to hours and could link fast and slow modules. Thus, a fast transient activation of the GPCR receptor that takes several seconds or less could induce a temporal YAP/TAZ response that lasts several hours. The time scales shown in Fig. 1 are based on previous computational studies of the dynamics of the modules (Cooling et al., 2007; Dupont et al., 2016), available experimental data (see Fig. 2), and model simulations.

In the following, we discuss the main signaling modules contributing to the Ca^{2+}-mediated YAP/TAZ regulation.

Module 1: GPCR activation—For the GPCR activation module, we used a previously developed mathematical model of Gq receptor cycling for non-excitable cells (Cooling et al., 2007). Reactions in the GPCR module were modeled by mass action kinetics (see Table 2). In GPCR module, ligand, angiotensin (Ang II) in this study, binds to cell-surface Gq receptor (GR) through reversible reactions causing a conformational change followed by the replacement of GDP with GTP on the Gqα subunit. Then, the Gqα subunit dissociates and stimulates the enzyme PLCβ. Phosphorylation of the active Gq receptor inactivates the receptor attenuating further signal transduction. To simulate cell response to Ang II, we modeled the ligand as a Heaviside step function with a nominal concentration of 0.1 μM. The adopted version of the GPCR module (Cooling et al., 2007) only becomes active for one cycle after ligand stimulation. Thus, to simulate cyclic activation of the GPCR module, we added reaction R6* (see Table 2) that resets the GPCR components to their initial states. The reaction R6*, modeled using mass action kinetics, is only active during the OFF period of cyclic ligand activation.

Module 2: IP_3-Ca^{2+} Module—In the IP_3-Ca^{2+} module, the active Gqα subunit (GqGTP) binds through the reversible reactions to the phospholipase C β (PLCβ) and activates it. However, GqGTP can also become inactivated to GqGDP without any potential to activate PLCβ. In addition to GqGTP, calcium ions (Ca^{2+}) are also necessary for the PLCβ

activation (Fig. 1C). In the resting condition, PLCβ-Ca^{2+} hydrolyzes phosphatidylinositol 4,5-bisphosphate (PIP2) and generates inositol 1,4,5-trisphosphate (IP_3) and diacylglycerol (DAG). However, after Gq stimulation with Ang II, PLCβ-Ca^{2+}-GqGTP hydrolyzes PIP2 at a higher rate to produce IP_3 and DAG.

Furthermore, after Ang II stimulation, the activation of phospholipase D (PLD) leads to phosphatidic acid (PA) accumulation, which increases DAG concentration through its phosphohydrolase (Sadoshima & Izumo, 1993). Thus, we included IP_3 and DAG accumulation mechanisms by PIP2 hydrolysis through PLCβ (adopted from ref.(Cooling et al., 2007)), Ang II-induced DAG accumulation by PA, and degradation of IP_3 and DAG in our model. All above reactions (R8-17) except PA-mediated activation of DAG were adopted from a mathematical model of IP_3 signaling (Cooling et al., 2007). Activation of DAG by Ang II through PA was modeled using mass action formula (R18-19). The model of Ca^{2+} buffering (R20) and CaM activation by four Ca^{2+} ions (R22) were adopted from a Ca^{2+} signaling mathematical model (Lukas, 2004).

In the model, Ca^{2+} levels in three ECM, cytosol, and ER compartments have been regulated by three fluxes through ER membrane, including J_{IP3R}, J_{SERCA}, and J_{ERleak}, and four fluxes through the plasma membrane, including J_{SOCE}, J_{PMCA}, J_{TRP}, and J_{PMleak}. We did not include voltage-gated Ca^{2+} channels and ryanodine receptors (RyRs), because we focus on non-excitable cells (Tajada & Villalobos, 2020).

J_{IP3R}, J_{SERCA}, $J_{PMCA,}$ J_{PMleak} and J_{ERleak} were adopted from a mathematical model of intracellular Ca^{2+}(Kowalewski et al., 2006). J_{IP3R} represents the release of Ca^{2+} from ER to the cytosol after activation of the IP_3R receptor by IP_3 (Baker et al., 2002; Kowalewski et al., 2006). Kowalewski et al. (2006) used De Young and Keizer's detailed model (De Young & Keizer, 1992) for the activation/deactivation of IP_3R channels capturing the biphasic behavior of the IP_3R channel opening at low and extremely high concentrations of Ca^{2+} and the CICR effect (Maurya & Subramaniam, 2007). J_{SERCA} and J_{PMCA} are Ca^{2+} pump fluxes and J_{ERleak} and J_{PMleak} represent the Ca^{2+} leak from ER and plasma membranes, respectively, and primarily regulate the resting level of Ca^{2+} in the cell.

Blocking SERCA by Tg disrupts Ca^{2+} homeostasis and causes the release of ER Ca^{2+} into the cytosol. Part of this Ca^{2+} enters mitochondria and results in mitochondrial fragmentation (Hom et al., 2007). As mitochondria and their Ca^{2+} variations are not in the scope of this study, the Tg-induced Ca^{2+} efflux from the cytosol into mitochondria and Ca^{2+} trap in mitochondria due to the mitochondrial fragmentation was modeled as part of the PM leak by using threshold function H(x) which capture a delayed decline in cytosolic Ca^{2+} transient as observed in experiment (Hom et al., 2007). H(x) is equal to x for x>0 and zero for x<=0. J_{SOCE} and J_{TRP} are important routes for Ca^{2+} flux from ECM into the cytosol in non-excitable cells. In SOCE, the depletion of ER Ca^{2+} triggers translocation of STIM1 to Orai1 channels at PM and Ca^{2+} influx into the cytosol by activated Orai1 channels (Dolan & Diamond, 2014; Huang et al., 2015). The overall process of Ca^{2+} depletion, STIM1 oligomerization, and translocation is a steep function of ER Ca^{2+} concentration, with a Hill coefficient in the range of 4 to 8 (Gudlur et al., 2018), and is included in our model by formulating J_{SOCE} as a Hill function of ER Ca^{2+}. Furthermore, the transient receptor

potential vanilloid-type 4 (TRPV4) channel is a matrix stiffness-sensitive Ca^{2+} channel that increases Ca^{2+} influx to cytosol in cells seeded on higher matrix stiffness (Sharma et al., 2017). We formulated J_{TRP} as a function of ECM stiffness like the formulation provided by Scott et al. (2021) to model the ECM stiffness effect on cell signaling.

Module 3: Kinases Module—Several kinases at Ca^{2+} downstream are known to mediate its effect on YAP/TAZ activity. As shown in Fig.1B, we identified the main players, including protein kinase C (PKC), CaMKII, protein kinase B (AKT), c-Jun N-terminal kinase (JNK), and protein tyrosine kinase 2 (Pyk2), from the literature that could contribute to YAP/TAZ regulation in a Ca^{2+}-dependent manner. PKC represents one of the primary effectors downstream of GPCRs (especially Gq receptors) and Ca^{2+}. PKC regulates a broad range of biological processes and can be classified into three sub-groups based on their activation mechanisms: 1) conventional PKCs (cPKC) that require both Ca^{2+} and DAG to be activated, 2) novel PKCs (nPKC) that are activated by only DAG, and 3) atypical PKCs (aPKC) that are independent of Ca^{2+} and DAG. CaMKII is another major kinase in Ca^{2+} signaling that regulates the activity of many species, including YAP/TAZ. As shown in Fig. 1C, CaMKII can control Actin Related Protein 2/3 complex (Arp2/3), LIM kinase (LIMK), AKT, and Pyk2 activity by phosphorylation. Arp2/3 and LIMK mediate CaMKII's impact on F-actin remodeling by regulating the G-actin to F-actin transition (Pollard et al., 2000; Zhao et al., 2012). AKT phosphorylates MST1/2 and inhibits its activity (Romano et al., 2014), and PyK2 links Ca^{2+} and CaMKII activity to the RhoA pathway (Ying et al., 2009). The c-Jun N-terminal kinase (JNK) also contributes to YAP activation by stiffness (Codelia et al., 2014). Activation of JNK by Ca^{2+} (Kushida et al., 2001) can regulate Hippo pathway activity by phosphorylation of LATS1/2 (Kodaka & Hata, 2015). The models of CaMKII activation by CaM and autophosphorylation and PKC activation by Ca^{2+} and DAG were adopted from the computational models of CaMKII signaling by Rangamani et al. (2016) and PKC signaling by Bhalla & Iyengar (1999), respectively. The mass action formula was used to model AKT, JNK, Pyk2, and F-actin-PKC forward reactions with the reaction rate linearly dependent on upstream activators (Scott et al., 2021). We used Michaelis-Menten kinetics to model AKT and JNK dephosphorylation by PP2A (Mukherjee et al., 2021).

Module 4: RhoA Module—In the RhoA module, focal adhesion kinase (FAK) links ECM stiffness and RhoA activation. An increase in ECM stiffness activates a cluster of integrins and their associated proteins, leading to FAK phosphorylation and subsequent activation of membrane-associated RhoA GTP (Palazzo et al., 2004). Rho-associated kinase (ROCK) and mammalian diaphanous-related formin (mDia) are downstream targets of RhoA. ROCK mediates RhoA activity to the myosin light chain (Myo) (Mammoto et al., 2004) as well as the F-actin module via LIMK(Wang et al., 2019b). Active mDia can facilitate F-actin polymerization(Yu et al., 2017). For modeling the RhoA module, we employed a modified version of the YAP/TAZ signaling model (Scott et al., 2021). We added Pyk2-dependent activation of RhoA and recalibrated certain parameters (Table 3) to capture ECM stiffness-induced variation of species in the RhoA module. We utilized steady-state data for the activity of species after an increase in ECM stiffness because of limited time-course data on ECM stiffness-induced variations in the biochemical activity of the species, which partly originates from the long time-scale of sensing of elevated stiffness by cells (Janmey et al.,

2020). The RhoA module reactions were adopted from a previously developed YAP/TAZ signaling model (Sun et al., 2016; Scott et al., 2021).

Module 5: F-actin Module—In the F-actin module, cytoskeletal reorganization represented by the transition between G-actin to F-actin and vice versa is modeled. The F-actin module also includes LIMK, cofilin, Arp2/3, and moesin-ezrin-radixin like (Merlin), which govern interactions between F-actin dynamics and the activity of other signaling modules in the model. Activation of LIMK by ROCK or CaMKII phosphorylates cofilin and decreases its inhibitory effect on G-actin to F-actin transition (Wang et al., 2019b). Arp2/3 complex mediates the effect of CaMKII activation on F-actin polymerization (Pollard et al., 2000; Rangamani et al., 2016). The NF2 gene product, Merlin, is a cytoskeletal protein that regulates LATS1/2 activation. As shown by Wei et al. (2020), Ca^{2+} elevation leads to Merlin ubiquitination and then promotes LATS1/2 activation by facilitating the interaction between Merlin and LATS1/2. Rearranged F-actin due to Ca^{2+} elevation provides the scaffold for the Hippo pathway regulation by Merlin (Wei & Li, 2021). The F-actin module was developed by adding Arp2/3 and Merlin activation mechanisms via mass action kinetics to a previously developed YAP/TAZ signaling model (Scott et al., 2021).

Module 6: Hippo-YAP/TAZ Module—The Hippo signaling module comprises several kinases that target YAP/TAZ. MST1/2 and LATS1/2 are the main species in the Hippo pathway. Following the sequential activation of MST1/2 and LATS1/2 through their phosphorylation, active LATS1/2 phosphorylates YAP/TAZ, leading to the sequestration of YAP/TAZ in the cytoplasm (Kodaka & Hata, 2015). If the Hippo pathway remains inactive, unphosphorylated YAP/TAZ translocates to the nucleus, where it binds to several cofactors, such as TEAD, that regulate the cell functions like growth and homeostasis through gene expression (Barra Avila et al., 2021). Furthermore, other mechanisms, such as the formation of stress fibers from myosin and F-actin, could facilitate the dephosphorylation of YAP/TAZ (Dupont et al., 2011). For modeling MST1/2 phosphorylation, we used the Michaelis-Menten formula, in which active PKC act as an enzyme to phosphorylate MST1/2. AKT acts as a competitive inhibitor of MST1/2 and is formulated by increasing the Km value, a common approach to model a competitive inhibition. We used a threshold function H(x) for MST1/2 activation by active cPKC-F-actin complex to qualitatively capture experimental observations on the timing of MST1/2 activation after Tg (Liu et al., 2019). Similarly, in modeling LATS1/2 phosphorylation, the Michaelis-Menten formula was used to include the effect of upstream activation (i.e., active MST1/2, nPKC, and Merlin) and inhibition signals (i.e., active JNK and cPKC) regulating LATS1/2 activity. We used Michaelis-Menten kinetics to model MST1/2 and LATS1/2 dephosphorylation by phosphatase (PP2A).

Several studies (Swift et al., 2013; Lomakin et al., 2017; Scott et al., 2021) demonstrated that species like LaminA and nuclear pore complexes (NPCs) could also regulate YAP/TAZ nuclear translocation. To model the LaminA and NPCs mechanisms of action, we utilized a previously published model (Scott et al., 2021), which considers the LaminA dephosphorylation rate as a function of cell cytosolic stiffness. In that model, cytosolic stiffness is estimated as a function of F-actin. Then, LaminA, in coordination with other cytoskeletal proteins like F-actin and myosin, can lead to the elevated nuclear YAP/TAZ

level by inducing nuclear stress and NPCs stretching resulting in lowered resistance of the NPC against the nuclear translocation of YAP/TAZ (Scott et al., 2021). The reactions regulating LaminA, Myo, NPC, and YAP/TAZ translocation were adopted from a previously developed YAP/TAZ signaling model (Scott et al., 2021) and modified to include the LATS1/2 interaction.

Non-modular species—In addition to the signaling modules discussed above, our model has other signaling species to capture cellular responses in Ca^{2+}-mediated YAP/TAZ activation. Protein Phosphatase 2A (PP2A) is a ubiquitously expressed serine-threonine phosphatase in cells that dephosphorylates many cellular species, including AKT, JNK, MST1/2, and LATS1/2 (Seshacharyulu et al., 2013; Hein et al., 2019). Previous studies demonstrated elevated phosphatase activity of PP2A in response to Ang II and thapsigargin, the model inputs, in different cell types (Huang et al., 1995; Li et al., 2003). We used Michaelis–Menten kinetics to model the dephosphorylation of species by PP2A in our model. Furthermore, to model the inhibitory effect of Tg on SERCA, we defined a hypothetical species that acts as the substrate of Tg (TGS) and controls SERCA flux (JSERCA). TGS also regulates the cytosolic Ca^{2+} efflux to ECM to artificially reproduce the delayed decline in cytosolic Ca^{2+} level due to Ca^{2+} efflux into mitochondria after mitochondria fragmentation by Tg (Hom et al., 2007).

2.3 Numerical methods

The model was constructed in VCell (Moraru et al., 2008). The system of deterministic ordinary differential equations was exported from VCell to MATLAB R2020b and was solved using the ‘ode15s’ solver for all numerical simulations with automatic time-stepping. The model was run for 100,000s without any inputs to reach the cell’s resting condition before conducting main simulations. We utilized a hybrid optimization algorithm comprising particle swarm optimization (Poli et al., 2007) and a fmincon Trust Region Reflective Algorithm (Byrd et al., 2000) to obtain estimated parameters in MATLAB with higher accuracy; see parameters indicated by “E” in the Ref. column of Tables 2-4. Steady-state values of model species were obtained at 100,000s when all species reached steady state. The model’s MATLAB code, including model species, parameters, reaction rates, and systems of ODEs, is available at https://github.com/mkm1712/ Calcium_YAP-TAZ. Cell geometric parameters used for model simulation include cytosolic volume (2300 μm^3), nuclear volume (550 μm^3), ER volume (425 μm^3), plasma membrane area (1260 μm^2), nuclear membrane (393 μm^2), and ER membrane area (21000 μm^2).

2.4 Model calibration to temporal and steady-state data

Out of the 156 kinetic parameters present in the model, 97 were obtained from previous models. To capture the dynamics of Ca^{2+}-mediated YAPTAZ signaling, kinetic parameters that were not available directly from previous experimental or computational studies were estimated from available experimental data manually curated from the literature. We obtained either quantitative time course and steady-state data from research articles with similar cell types, assays, and experimental conditions with a preference for data from non-excitable endothelial cells. However, considering the limited data availability, a few sets of smooth muscle data were also included in the model calibration. Figure 2 illustrates

the comparison between model simulation results and experimental data for various model species. We utilized the scatter index (SI), which is the root mean square error (RMSE) normalized to the mean of measured data, to evaluate the goodness of fit between *in silico* results and calibration data.

We conducted two types of calibrations – a comparison of the dynamics of concentrations of different species in the model for chemical stimuli (Fig. 2A) and a comparison of the steady-state response of some species in the model as a function of substrate stiffness (Fig. 2B). We show that the model can capture the dynamics of signaling species with different time scales after GPCR (Ang II) and thapsigargin (Tg) stimulations. All experimental and *in silico* data were normalized to their maximum values to enable direct comparison. Figures 2A-I&II display simulated IP_3 and cytosolic Ca^{2+} transient levels after Ang II stimulation reproducing experimental data with a peak in 20 seconds and returning to the resting level after 5 min. These transient responses indicate fast dynamics of the IP_3-Ca^{2+} module that reaches a steady state in 5-10 mins. The IP_3 dynamics and its relaxation time is mainly regulated by the Gq receptor phosphorylation rate (Cooling et al., 2007). In the case of Ca^{2+}, given the considerable number of regulators and their interactions, determining key processes is challenging. However, sensitivity analysis results could provide some insights on the major regulators of Ca^{2+} transient that are addressed in section 2.5.

For DAG and PA, we observed a sustained increase in their concentrations after Ang II stimulation (Figs. 2C-D) with a steady-state level after 15 min. While the PLCβ-mediated mechanism of DAG and IP_3 production are the same, we observe a slower rise time for DAG due to the slower dynamics of PA-mediated DAG production. Moreover, DAG mainly follows PA in its relaxation. We also included Tg in the model to simulate direct regulation of Ca^{2+} to prevent potential interference of Ca^{2+}-independent pathways in regulating YAP/TAZ response. In contrast to Ang II, Tg-induced cytosolic Ca^{2+} transient in cells had a higher steady-state level than resting Ca^{2+} level due to the release of a significant amount of Ca^{2+} from ER to the cytosol (Fig. 2E). While a large portion of this Ca^{2+} is transported into mitochondria and ECM (Hom et al., 2007), the remaining Ca^{2+} in cytosol leads to an elevated steady-state level of cytosolic Ca^{2+} after Tg stimulation (Kline & Kline, 1992; Zhong et al., 2016). Tg-induced Ca^{2+} dynamics (time scale of 30 mins) is slower than Ang II-induced Ca^{2+} because of 1) slower dynamics of SERCA and SOCE compared to IP_3R resulting in higher Ca^{2+} rise time after Tg, and 2) slow process of Ca^{2+} efflux from the cytosol into mitochondria (Hom et al., 2007) leading to higher relaxation time. Furthermore, Ang II induces a fast rising to the peak (2-5 min) in JNK, Pyk2, and AKT (Figs. 2F-H). However, their slow dynamics in return to baseline (or lower) due to slow dephosphorylation by phosphatases (PP2A and PP1) result in a long relaxation time (1-5 hours) which put the kinases in the intermediate time scale (dozen minutes to 1-2 hours). Interestingly, JNK and AKT have steady-state levels lower than their initial resting levels after Ang II stimulation, partly because of an Ang II-induced increase in PP2A phosphatase activity (Fig. 2I).

To develop a Ca^{2+}-mediated YAP/TAZ signaling model capable of capturing various experimental settings, including potential changes in ECM stiffness, we utilized steady-state data of ECM stiffness as input to estimate some parameters in the RhoA and YAP/TAZ modules. Figures 2B-I and II illustrate the increase in the RhoAGTP (Lampi et al., 2016)

and active myosin (Myo*) (Lampi et al., 2016) levels, respectively, in response to a higher ECM stiffness. RhoAGTP reaches its saturation level for ECM stiffness greater than 100 kPa, making its downstream target, including YAP/TAZ, insensitive to substrate (ECM) stiffness larger than 100 kPa. As suggested by some studies (Sun et al., 2018; Scott et al., 2019, 2021; Jiang et al., 2022), ECM stiffness-induced alteration in the cell cytoskeleton and stiffness is responsible for many variations in cell signaling and phenotypic changes. Thus, in our model, the parameter (Ecyt), a function of ECM stiffness that reflects cellular stiffness, controls LaminA activation. Figures 2B-III and IV compare *in silico* and experimental variations in cell stiffness (Solon et al., 2007) and LaminA activity (Swift et al., 2013) for various ECM stiffnesses, respectively. Finally, in Fig. 2B-V, we compared the model results with six different experimental datasets (Das et al., 2016; Caliari et al., 2016; Barreto et al., 2017; Elosegui-Artola et al., 2017; Han et al., 2018; Lee et al., 2019) illustrating ECM stiffness-induced variations in YAP/TAZ N/C (nuclear to cytosolic ratio) as a measure of YAP/TAZ activity. These extensive calibration curves establish confidence in our choice of kinetic parameters and model formulation for both chemical and mechanical inputs.

2.5 Parametric sensitivity analysis

Next, we determine the sensitivity of the model to different parameters. We chose to conduct a global sensitivity analysis because a local sensitivity analysis has limitations in capturing nonlinear interactions between species in a complex network such as Ca^{2+}-mediated YAP/TAZ signaling. Therefore, we performed a Morris global sensitivity analysis (Khare et al., 2015) by changing all model parameters (+/− 50% around nominal value), including kinetic and geometric parameters, as well as the initial conditions to compute their global effects on the YAP/TAZ N/C ratio after Tg and Ang II stimulation. We calculated the Morris sensitivity measures including the Morris index (μ^*) and standard deviation (σ) for each parameter in the model. The Morris elementary effects method is a proper screening method used to determine model output sensitivity to variations in its parameter in the case of large-scale network models with numerous parameters (Khalilimeybodi et al., 2020; 2022). To conduct the sensitivity analysis, first, we generated Morris sampling data through the EE sensitivity package developed by Khare et al. (2015) with the “Sampling for Uniformity” strategy, oversampling size of 300, input factor level of 16, and trajectory number of 16. By using the Morris method, we can find if the effect of changes in a parameter on the model output is important or negligible, linear or nonlinear, and with or without interactions with other parameters (Balesdent et al., 2016). The μ^* and σ are the mean of the absolute values and standard deviation of the elementary effects (EEs) (more detail in Khare et al., 2015). While higher μ^* means a greater influence of the parameter on model output, higher σ indicates greater interaction with other parameters meaning a more nonlinear effect on model output.

In Fig 3, we show the model sensitivity analysis results for Tg (panel A) and Ang II (panel B) contexts involving the parameters with high sensitivity scores ($\mu^*>0.05$). According to the results, parameters controlling Ca^{2+} channels and pumps, especially SERCA and PMCA, have the highest impact on cell response, followed by geometric and other IP_3-Ca^{2+} module parameters. In Fig. 3, cell geometry parameters are the size and area of the model

compartments, such as the cytosolic compartment size or plasma membrane area. Given the central role of Ca^{2+} dynamics in both Ang II and Tg contexts, most parameters have similar impacts on cell response in both contexts. However, the parameters that regulate cPKC and PP2A are more specific to Tg and Ang II contexts, respectively.

A main feature of the Morris sensitivity analysis is its capability to determine parameters (reactions) with a more non-linear effect on model output through σ measure. According to Fig. 3, parameters regulating SERCA, PMCA, SOCE, PLCβ, IP3, and DAG have the highest standard deviation σ. Higher σ indicates a greater level of interactions between these parameters (reactions) with other parts of the YAP/TAZ signaling network, which makes them the potential drivers of nonlinearity in the whole system. Considering the reactions formula (Tables 2-4), JIP3R, JSERCA, JPMCA, JSOCE, CaMKII, Merlin, LaminA, and NPC could contribute to the nonlinearity of the system. However, given the upstream position of Ca^{2+} fluxes in the YAP/TAZ network, their effect on the whole system dynamics would be greater, as confirmed by the sensitivity analysis results. Moreover, as shown in Fig. 3, many important parameters determined by sensitivity analysis have a non-monotonic relationship with the YAP/TAZ activity (shown by blue stars) which means that in a range of parameter space, an increase in the parameter results in elevated YAP/TAZ activity and on another range, it diminishes YAP/TAZ activity. As we expect more parameters with a monotonic effect (orange dot) on the model output in a network with a few crosstalk, this result indicates a considerable level of crosstalk between network species in the YAP/TAZ network, which could be another driver of nonlinearity in the model input-output relationship.

3 Results

According to previous experimental observations (Wei & Li, 2021), there are distinct responses of YAP/TAZ to Ca^{2+} in different experimental settings. This dissimilarity in Ca^{2+}-mediated YAP/TAZ response may originate from inherent differences in dynamics and context-dependency of the complex signaling network regulating the YAP/TAZ (Fig. 1A). In this study, by employing the compartmental ODE model of the Ca^{2+}-mediated YAP/TAZ signaling, we investigate how the dynamics of Ca^{2+} and signaling modules in the Ca^{2+}-mediated YAP/TAZ network and changing the cell context including cell stimuli (type and frequency), and cell type (properties of Ca^{2+} handling proteins) could lead to diverse responses observed for Ca^{2+}-YAP/TAZ relationship.

3.1 Dynamics of Ca^{2+} and Hippo-YAP/TAZ pathway in response to Ang II and Tg stimulation

We first investigate the dynamics of the Hippo pathway and YAP/TAZ mediated by Ca^{2+}. Our input was Tg (1 μM) or Ang II (0.1μM), and stiffness was maintained at zero kPa. Changes in cytosolic Ca^{2+} after Ang II and Tg stimulations are illustrated in Fig. 4A. While Ang II induces a fast Ca^{2+} transient with no increase in steady-state Ca^{2+} level, Tg stimulation leads to a slow Ca^{2+} transient with an elevated level of Ca^{2+} at steady-state. Response of the Hippo pathway, including its core components: MST1/2 and LATS1/2, to changes in cytosolic Ca^{2+} after Ang II and Tg stimulations is displayed in Fig. 4B.

MST1/2 is largely dephosphorylated in resting conditions exhibiting only 2-3% of its maximal activity (Galan & Avruch, 2016). While no rich time course data is available for MST1/2 after Tg or Ang II stimulation, experimental observations indicate a significant increase in MST1/2 phosphorylation after 30 min stimulation with Tg (Liu et al., 2019) and sustained activity of MST1/2 in the presence of Ca^{2+} (Lee et al., 2008), possibly due to its autophosphorylation (Praskova et al., 2004; Galan & Avruch, 2016). Simulations from the model indicate an increase in MST1/2-p from a 2% resting level, a peak between 30 min and 1 hour. and a slow decline (2-5 hours) to a steady-state level higher than its initial level. The model indicates a higher peak value and decline rate for MST1/2 activity after the Tg stimulus (red curve) compared to Ang II (blue curve).

We also found that activation trends for LATS1/2 and MST1/2 are similar for both stimuli (Fig. 4B). However, the LATS1/2-p production rate is much larger than MST1/2-p due to multiple upstream activators. Interestingly, in contrast to MST1/2-p, LATS1/2-p has only a higher steady-state level after Tg stimuli when compared to the initial concentration. In the case of Ang II stimulation, the LATS1/2-p steady-state level is lower than its initial level, indicating that Ang II has an inhibitory effect on LATS1/2 in the long term, similar to what has been observed in experimental studies (Yu et al., 2012; Zhang et al., 2021). In the context of Tg stimulus, experimental data indicate an increase in LATS1/2 activity with a peak at 30 min and a fast decline to the initial level (Wei et al., 2020). However, the model predicts a higher LATS1/2-p steady-state level than experimental data (Wei et al., 2020), partly originating from a higher steady-state level of cytosolic Ca^{2+} after Tg in the simulations.

While some studies indicate a higher Ca^{2+} level after Tg[45], others showed no difference between the initial and steady-state levels of cytosolic Ca^{2+} after Tg stimulation, which could explain low long-term LATS1/2 activity in some experiments (Wei et al., 2020). Next, we study the impact of Ang II and Tg on YAP/TAZ activity, reported as YAP/TAZ N/C ratio (Sun et al., 2016; Scott et al., 2021). As shown in Fig. 4C, after a small and fast uprise, YAP/TAZ N/C ratio decreases to its minimum (~30-40 min for Ang II and 60-70 min for Tg) and then rises to reach its steady-state value after 10 hours. While both Ang II and Tg result in a transient elevation in Ca^{2+} level, due to the difference in the steady-state level of Ca^{2+} between Ang II and Tg (Fig. 4A), their YAP/TAZ activities in the long term are significantly different, indicating the important role of steady-state Ca^{2+} level in regulating Ca^{2+}-YAP/TAZ relationship in the long term (Wei & Li, 2021).

3.2 Context-dependent contribution of upstream regulators to Hippo-YAP/TAZ activity

We next explored the role of upstream regulators from different signaling modules, including cPKC, AKT, CaMKII, RhoA, F-actin, DAG, JNK, nPKC, and LaminA, on the dynamics of the Hippo pathway and YAP/TAZ. To do this, we simulated the removal of each regulator's effect on its downstream targets by setting the regulator's rate of variations equal to zero. Then, we simulated the variations of MST1/2-p, LATS1/2-p, and YAP/TAZ N/C levels in both Ang II and Tg contexts. This analysis allowed us to determine the degree that each upstream pathway impacts the Hippo pathway and YAP/TAZ activity. We determined the impact of removing each regulator on time to peak or trough (Fig. 4D) and

relaxation time (Fig. 4E) for MST1/2-p, LATS1/2-p, and YAP/TAZ activity after Tg and Ang II stimulation. Removal of cPKC or DAG makes the dynamics of Hippo and YAP/TAZ faster by decreasing peak/trough and relaxation times. We then plotted the steady-state concentrations and peak values of MST1/2-p and LATS1/2-p after removing each upstream regulator effect for both Ang II and Tg stimuli in Fig. 4F. We found that removing the contribution of cPKC decreases active MST1/2 and LATS1/2 steady-state levels as well as active MST1/2 peak levels in both contexts. However, cPKC or DAG removal increases the active LATS1/2 peak level. In addition, by comparing steady-state levels of YAP/TAZ activity after removing the contribution of each regulator (Fig. 4G), we found that PKC removal also results in higher steady-state YAPTAZ activity. In brief, Ca^{2+}-induced increase in cPKC or DAG activity could make the Hippo and YAP/TAZ dynamics slower and leads to lower YAP/TAZ activity in the long term through elevating MST1/2 and LATS1/2 steady-state phosphorylation.

CaMKII is a known Ca^{2+} downstream target affecting many signaling pathways (Iribe et al., 2006; Zhao et al., 2012; Bouallegue et al., 2013). Our model predicts that removing the effect of CaMKII reduces MST1/2-p and LATS1/2-p peak levels only after Tg, not Ang II (Fig. 4F). This stimulus-specific response is more apparent in its effect on Hippo pathway dynamics. While abolishing the CaMKII contribution reduces the peak times of the Hippo pathway in the Tg context, it slightly increases these times in the Ang II context (Fig.4D-E). It also significantly increases Hippo pathway relaxation times for Tg stimulus without any significant impact on relaxation times for Ang II stimulus. Regarding YAP/TAZ, CaMKII contribution's removal only significantly decreases the trough and relaxation times for the Tg stimulus and has no effects on YAP/TAZ steady-state levels for both stimuli (Fig.4D-G). Thus, the model predicts that CaMKII contribution to Hippo and YAP/TAZ activity is more pronounced in cell stimulation by Tg rather than Ang II. Moreover, the CaMKII impact is more limited to Hippo and YAP/TAZ temporal dynamics than steady-state activities.

F-actin is a key cytoskeletal component implicated in the regulation of YAP/TAZ nuclear translocation (Das et al., 2016; Dasgupta & McCollum, 2019). Removal of F-actin contribution to Ca^{2+}-mediated Hippo-YAP/TAZ pathway activity results in the decrease in Tg-induced MST1/2-p and LATS1/2-p peak and steady-state levels and Ang II-induced LATS1/2-p peak level (Fig.4F). It also diminishes peak/trough times of the Hippo-YAP/TAZ pathway in the Tg context and increases peak times of the Hippo pathway in the Ang II context (Fig. 4D). The removal of F-actin contribution increases relaxation times of MST1/2-p and YAP/TAZ only in Tg context. Besides, it only decreases Tg-induced YAP/TAZ steady-state level (Fig. 4G). In summary, F-actin can participate in both the inhibition and activation of YAP/TAZ. On one hand, higher F-actin increases YAP/TAZ nuclear translocation through cytosolic stiffness modulation. On the other hand, it can contribute to YAP/TAZ inhibition by cPKC-dependent activation of LATS1/2. Given these two opposite effects, the model predicts that F-actin in the long-term activates YAP/TAZ after a Tg-induced increase in Ca^{2+}.

LaminA controls YAP/TAZ nuclear translocation by inducing the stretching of NPCs resulting in their lower resistance against YAP/TAZ nuclear import. As expected, removal of LaminA contribution only affects YAP/TAZ dynamics but not MTS1/2 or LATS1/2

dynamics. Lack of LaminA changes in our model decreases the time to trough for YAP/TAZ and the YAP/TAZ steady-state level only after Tg stimulus and elevates Tg-induced YAP/TAZ relaxation time. While other regulators like AKT, RhoA, JNK, and nPKC contribute to the dynamics of the Hippo-YAP/TAZ pathway at some level (Figs. 4D-F), their effects are significantly lower than regulators discussed above. In summary, we find that while the dynamics of YAP/TAZ falling to its trough is mainly controlled by phosphorylation, nuclear translocation regulates its rise to the steady-state level.

3.3 Ca^{2+} temporal dynamics govern the switching of the Ca^{2+}-YAP/TAZ relationship

One of the potential causes of diversity in the Ca^{2+}-YAP/TAZ relationship is the significant variation of the cytosolic Ca^{2+} dynamics observed in different cell contexts (e.g., cell types and experimental settings) (Kang & Othmer, 2007; Dupont et al., 2016; Wei & Li, 2021). These variations are occasionally unrecognizable due to the noise or Ca^{2+} waves but may result in distinct downstream responses like Ca^{2+}-YAP/TAZ diverse relationships. In this section, we explore how variations in Ca^{2+} transient in different cells may lead to Ca^{2+}-induced activation or inhibition of YAP/TAZ. We generated several artificial Ca^{2+} transients by perturbing two model parameters with high impacts on Ca^{2+} transient. These parameters are Michaelis constant (Km) for PMCA function and Hill power (n) for SERCA function. Figures 5A-I, III illustrate the Ca^{2+} transient response in the Tg context by altering n (SERCA) and Km (PMCA) around their nominal values of 1 and 0.2 μM, respectively. While altering n (SERCA) significantly elevates Ca^{2+} initial resting level and reduces the peak time, its effect on Ca^{2+} steady-state level, relaxation time, and the peak value is negligible (Fig. 5A I). Therefore, we observed significant reduction in initial YAP/TAZ N/C ratio and changes in YAP/TAZ dynamics in the first hour after stimulation (Fig. 5A-II). However, YAP/TAZ steady-state level and dynamics at longer times are nearly unchanged. This may explain the divergent YAP/TAZ activity after the transient elevation of cytosolic Ca^{2+} in the cells. According to results, a Ca^{2+} transient with (solid red and dotted blue lines in Fig. 5A-I) and without (dashed black line in Fig. 5A-I) steady-state increase in Ca^{2+} concentration could lead to the opposite direction of changes in YAP/TAZ steady-state activity (Fig. 5A-II). Thus, the ratio of steady-state to the initial level of cytosolic Ca^{2+} during Ca^{2+} stimulation could predict the Ca^{2+}-YAP/TAZ relationship in the cell.

Varying Km-PMCA has a significantly different impact on the Ca^{2+} transient compared to n-SERCA. Increase in Km-PMCA shifts the entire Ca^{2+} transient response to higher Ca^{2+} levels with a relatively small decrease in peak time and no significant changes in relaxation times and the ratio of steady-state to the basal level of cytosolic Ca^{2+} (Fig. 5A-III). The resultant YAP/TAZ activity shifts in an opposite direction by moving toward a lower YAP/TAZ N/C ratio and higher trough time; see changes from the dotted blue line to the solid red line in Fig. 5A-IV. However, a further increase in Ca^{2+} level, from red line to dashed black line (Fig. 5A-III), led to a switch in the Ca^{2+}-YAP/TAZ relationship from inhibition to activation and increased YAP/TAZ steady-state and decreased the trough time (Fig. 5A-IV). This result predicts that the absolute level of cytosolic Ca^{2+} could affect the Ca^{2+}-YAP/TAZ relationship.

Increasing n-SERCA in the Ang II context leads to an increase in relaxation time and significant elevation of Ca^{2+} initial and steady-state levels, which decreases Ca^{2+} amplitude (Fig. 5B-I). As shown in Fig. 5B-II, this change in Ca^{2+} transient results in switching the Ca^{2+}-YAP/TAZ relationship like Fig. 5A-IV. However, in contrast to Fig. 5A-IV, the YAP/TAZ trough time in Fig. 5B-II is not significantly changed. On the other hand, increasing Km-PMCA in the Ang II context elevates Ca^{2+} amplitude significantly while slightly increasing Ca^{2+} initial and steady-state levels. This change in Ca^{2+} transient, as shown in Fig. 5B-IV, leads to a smooth shift in Ca^{2+}-YAP/TAZ relationship from inhibition to activation by decreasing YAP/TAZ N/C initial level more than its steady-state level.

These results confirm the previous model predictions on the contribution of higher Ca^{2+} levels to the change in the Ca^{2+}-YAP/TAZ relationship. However, the difference between YAP/TAZ responses after the Ang II stimulus (Fig. 5B) despite similar Ca^{2+} transient predicts the high sensitivity of YAP/TAZ temporal response to Ca^{2+} transient characteristics such as Ca^{2+} amplitude. In summary, model results indicate a significant role of Ca^{2+} temporal dynamics, amplitude, and steady-state level in Ca^{2+}-YAP/TAZ relationship. All four categories of artificial Ca^{2+} transients (Figs. 5A-I, III, 5B-I, III) alter Ca^{2+}-YAP/TAZ relationship from inhibition to activation through different process, some through a switching event (Figs. 5A-IV, 5B-II) and some through a smooth change (Figs. 5A-I, 5B-IV).

To explore the origin(s) of the switching phenomenon that may explain divergent Ca^{2+}-YAP/TAZ relationships observed in some experiments, we screened the variations of all signaling components in the model and found the bistable CaMKII steady-state activity as a potential cause. As shown in Figures 5C and D, various Ca^{2+} transients in the Tg and Ang II contexts lead to different CaMKII activities. In the cases where CaMKII autophosphorylation is not significant, the CaMKII transient follows the Ca^{2+} transient timing and reduces to its low value after the decline in the Ca^{2+} level (red line). However, in cases with strong CaMKII autophosphorylation, CaMKII remains at its high activity level after the decline in Ca^{2+} level (dashed black line). Comparing the time course of CaMKII activity for solid red line and black dashes line in Figs. 5C,D, suggests that the potential impact of CaMKII on the Ca^{2+}-YAP/TAZ relationship can be detected after 1 hour for the Tg context and 5 min for the Ang II context and might explain the shift in the YAP/TAZ trough toward shorter times in Fig. 5A-IV. In brief, results predict that if we have a bistable response of CaMKII (high or low steady-state activity based on Ca^{2+} temporal dynamics) as observed in some cell types (Michalski, 2013; Yasuda et al., 2022), specific changes in Ca^{2+} transient could switch the Ca^{2+}-YAP/TAZ relationship.

3.4 YAP/TAZ exhibits a non-monotonic response to periodic GPCR activation

Repetitive transient increases in IP_3 and cytosolic Ca^{2+} after GPCR stimulation can be seen in a broad range of non-excitable cells (Harootunian et al., 1991). However, it is not clear how these periodic activations of the IP_3-Ca^{2+} module affect the YAP/TAZ pathway. To explore the sensitivity of YAP/TAZ activity to the frequency of IP_3-Ca^{2+} module activation, we simulated Ang II-induced activation of the IP_3-Ca^{2+} module using a square wave input (Ang II) at various periods (T) from 2 days to 10 min. Each period involves two equal

times for cell activation and rest. For example, in a 2 days period, we have one day of Ang II stimulation and one day of cell rest. In the 2 days period, there is sufficient time for YAP/TAZ signaling components to reach their steady-state level without any frequency-related impact on YAP/TAZ (Fig. 6A). However, by lowering the period (T) from 2 days to 10 min, we observed a steady decrease in YAP/TAZ amplitude (difference between the mean value and max/min in each period) and a non-monotonic response for YAP/TAZ mean activity (Figs. 6B-C). Lowering the period (T) from 2 days to 2 h elevated the YAP/TAZ mean activity. But a further decrease from 2 h to 10 min reduced YAP/TAZ mean activity resulting in a maximum for YAP/TAZ mean activity in the 2 h period. By comparing steady-state levels of YAP/TAZ between 2 days and 10 min, we can predict that increasing the frequency could change the direction of the Ca^{2+}-YAP/TAZ relationship in the Ang II context from a positive relationship to a negative one.

To investigate which signaling mediators participate in this frequency-dependent YAP/TAZ response, we simulated the response of main mediators in the model to periodic GPCR activation by Ang II for 2 days, 2 h, and 10 min periods. All mediators showing significant frequency-dependent effects are illustrated in Figs.6D-I. The JNK-p and AKT-p inhibit the Hippo pathway and can thus be considered activators of YAP/TAZ. As shown in Figures 6D-E, a decrease in period (T) reduces the amplitude of both JNK-p and AKT-p. However, JNK-p and AKT-p responses are completely different regarding the direction of changes in the mean activity and period threshold. Based on the results, we estimated a period threshold between 2 days and 2h for JNK-p and a lower period threshold between 2h and 10 min for AKT-p. Pyk2-p activates the RhoA pathway and then F-actin; it can be considered a YAP/TAZ activator (Fig. 1C). A decrease in period (T) results in a lower amplitude and higher mean value for Pyk2-p (Fig. 6F).

cPKC has a bidirectional effect on the Hippo pathway (Urtreger et al., 2012; Gong et al., 2015). However, our results (Fig. 4F) indicated a dominant cPKC inhibitory action on YAP/TAZ steady-state activity. As shown in Fig. 6G, a decrease in the period T elevates the mean activity of cPKC without significantly changing its amplitude. LATS1/2, as a direct inhibitor of YAP/TAZ, significantly contributes to its frequency-dependent response. As shown in Fig. 6H, the LATS1/2-p response is the opposite of the YAP/TAZ response in terms of mean activity. Finally, LaminA, an activator of YAP/TAZ that facilitates its nuclear translocation, exhibits a slight increase in the mean activity after a decrease in period T.

In summary, model results predict a non-monotonic YAP/TAZ activity in terms of period T due to the distinct response of YAP/TAZ upstream regulators to periodic GPCR activation. The model predicts that while frequency-induced inhibition of JNK and activation of cPKC favor a decrease in YAP/TAZ activity, activation of AKT, Pyk2, and LaminA tend to increase YAP/TAZ activity. Accordingly, the results predict the dominance of cPKC and JNK impact on YAP/TAZ in longer periods and AKT, Pyk2, and Lamin A impacts in shorter periods. Results also confirmed a significant role for LATS1/2 in mediating YAP/TAZ frequency-dependent response.

4. Discussion

Here, we developed a prior knowledge-based network model of Ca^{2+}-mediated YAP/TAZ signaling to examine how different temporal dynamics of signaling species contribute to distinct YAP/TAZ responses observed in experiments. The model comprises seven signaling modules and their crosstalk that interact with Ca^{2+} and transduce biochemical (Ang II) and biomechanical signals (ECM stiffness) to YAP/TAZ. The identified signaling modules include GPCR, IP_3-Ca^{2+}, Kinases, RhoA, F-actin, Hippo, and YAP/TAZ module. The model captures both time course and steady-state data available in the literature. By employing our model, we make a series of experimentally testable predictions. First, we predicted that while both Ang II and Tg stimuli decrease YAP/TAZ activity in the short time, AngII activates YAP/TAZ in the long term in contrast to Tg. Second, we identified the major mediators of Ca^{2+}-induced YAP/TAZ activation (e.g., cPKC, DAF, CaMKII, F-actin, and LaminA) and predicted their context-specific contribution to YAP/TAZ dynamics and steady-state behavior. Third, we predicted how variations in Ca^{2+} transients in different cell contexts might lead to the controversial Ca^{2+}-YAP/TAZ relationship observed in experimental data. We predicted the relationship between basal and steady-state cytosolic Ca^{2+} levels and direction of changes in Ca^{2+}-induced YAP/TAZ activity, the contribution of Ca^{2+} amplitude on YAP/TAZ temporal response, and the significant role of CaMKII bistability in switching Ca^{2+}-YAP/TAZ relationship. Finally, we predicted a non-monotonic YAP/TAZ activity in response to periodic GPCR activation because of distinct frequency-dependent responses of YAP/TAZ upstream regulators.

4.1 The cPKC and Hippo core kinases integrate signals with distinct temporal scales in YAP/TAZ regulation

Cells experience and respond to numerous biochemical and mechanical stimuli during their lifetime. Although multiple mechanisms have been identified for cell mechanotransduction, a major part of these mechanisms act through ECM and lead to cell cytoskeletal remodeling in the order of several hours to days (Kolahi & Mofrad, 2010). Unlike mechanical activators like ECM stiffness, a majority of biochemical stimuli like GPCR agonists are considered fast inputs resulting in receptor activation and downstream signaling in the order of seconds to minutes (Yu et al., 2012; Wang et al., 2019a). For proteins like YAP/TAZ sensitive to both fast and slow stimuli (Piccolo et al., 2014; Totaro et al., 2018), upstream regulators that integrate signals with different time scales are necessary. In Ca^{2+}-mediated YAP/TAZ signaling, we predict that cPKC and core Hippo pathway components (MST1/2 and LATS1/2) may play this role. Removing the effects of cPKC activation in Ang II and Tg contexts significantly shifts the Hippo-YAP/TAZ dynamics to a faster response with a lower transient peak for Hippo pathway components and higher steady-state activation of YAP/TAZ.

Inhibition of cPKC as one of the key effectors downstream of GPCR can activate or inhibit YAP/TAZ in a context-dependent manner (Gong et al., 2015; Wang et al., 2019b; Wei & Li, 2021). cPKC inhibition effectively blocked dephosphorylation of YAP/TAZ by acetylcholine (Gq11-coupled receptor agonist) in U251MG cells (Gong et al., 2015). It also blocked amlodipine- or ionomycin-induced YAP/TAZ phosphorylation in LN229 cells (Liu

et al., 2019). In addition to cPKC, the sustained activity of the Hippo pathway, especially MST1/2, after Ang II significantly contributes to the YAP/TAZ sensitivity to fast GPCR signals. Furthermore, AKT has the potential for integrating upstream signals, as shown in Fig. 6. However, AKT removal did not noticeably affect MST1/2 and LATS1/2 peak and steady-state levels based on model results. Based on our predictions, we can hypothesize that while MST1/2 phosphorylation by AKT can decrease MST1/2 activity (Romano et al., 2014; Galan & Avruch, 2016), because of the large unphosphorylated portion of MST1/2 in cells (Galan & Avruch, 2016), Ca^{2+}-induced AKT activation cannot practically limit activation of MST1/2 by cPKC and F-actin.

4.2 CaMKII autonomous activity controls Ca^{2+}-YAP/TAZ bidirectional relationship

CaMKII is an auto-phosphorylating kinase that acts as major Ca^{2+} signaling downstream in cell physiology and pathology (Michalski, 2013). Autophosphorylation of CaMKII could lead to Ca^{2+}/CaM-independent (autonomous) kinase activity that can last 30 min or longer after a short-term transient increase in cytosolic Ca^{2+} concentration (Zhabotinsky, 2000). To cover Ca^{2+} signaling in various cell types, our model considers both Ca^{2+}/CaM-dependent and autonomous activation of CaMKII (Table 3). As shown in Fig. 5, a change in the Ca^{2+} dynamics could alter the direction of changes in Ca^{2+}-YAP/TAZ interaction from Ca^{2+}-induced inhibition of YAP/TAZ to activation, and CaMKII autonomous activation could mediate this switching process.

In the context of Tg stimulation, the model predicts a high activity for CaMKII starting from ~5 min and ending before one hour. Likewise, Timmins et al. (Timmins et al., 2009) illustrated that after Tg stimulation, CaMKII rises to its maximum in 5 min and declines to its initial level in 30 min. Zhong et al. (Zhong et al., 2016) also reported Tg-induced CaMKII activation with a steady increase till 30 min and then return to the resting level before one hour. For the Ang II context, the model predicts a rise to maximum CaMKII activity in 1 min and a return to the initial level in less than 5 min. Zhu et al. (Zhu et al., 2000) showed similar activation of CaMKII after Endothelin-1, a Gq activator, with maximum CaMKII activity in 1 min and returning to the initial level in 6 min. However, the Ang II-induced CaMKII transient response can be switched to a sustained response (Fig. 5D) with high CaMKII activity even after one day (Zhou et al., 2016). Given the significant variability between cell types in Ca^{2+} dynamics and CaMKII autonomous activity, the model results predict that in the cells with potential CaMKII autonomous activity, the context-dependent duration of high CaMKII activity could alter the Ca^{2+}-YAP/TAZ relationship from one context to another (Wei & Li, 2021). In the cells where CaMKII autonomous activity is not significant, we expect a more robust cell response in terms of the Ca^{2+}-YAP/TAZ relationship to variations in Ca^{2+} transient, especially for changes reflecting a shift of Ca^{2+} transient to higher or lower concentrations (Fig. 5A-III).

4.3 The model predicts Ca^{2+}-YAP/TAZ distinct relationships in experiments

The Ca^{2+}-YAP/TAZ relationship is controversial. Multiple experimental studies reported both inhibition and activation relationship between Ca^{2+} and YAP/TAZ reviewed by Wei and Li (2021). To explore the cell response and Ca^{2+}-YAP/TAZ relationship in each study, we simulated various experimental conditions by the model. The model results are compared

with experimental data in Table 5. In the first study, authors knocked out the TPCN2 gene in CHL1 and B16-F0 (murine primary melanoma) cell lines and observed activation of YAP/TAZ in the cells (D'Amore et al., 2020). They suggested the contribution of Orai 1 and PKCβ in the activation of YAP/TAZ, given the significant decrease in their expressions in the knockout cells. We simulated this experiment with a 30% decrease in $Ymax_{SO}$ value (see Table 2, J_{SOCE}) and a 90% decrease in cPKC initial concentration (Table 1) to reproduce reported experimental changes in Orai1 and cPKC expression (D'Amore et al., 2020). As shown in Table 5, the model predicts an increase in YAP/TAZ activity similar to experimental data. Interestingly, while simulating each perturbation at a time increased the YAP/TAZ N/C ratio, applying both perturbations together yielded less of an increase in YAP/TAZ N/C than just cPKC knockdown, indicating the non-linearity of cell response in Ca^{2+}-mediated YAP/TAZ activity.

In the second study, Dang et al. (2019) showed that overexpression of Ca^{2+}-ATPase isoform 2 (SPAC2) in breast cancer cells elevates baseline Ca^{2+} and YAP phosphorylation and decreases YAP/TAZ activity. Consistent with the experiment, the model predicts an increase in YAP phosphorylation and a decrease in YAP/TAZ activity after a 30% increase in baseline Ca^{2+} by applying higher extracellular Ca^{2+}. The third study demonstrates that upregulation of Ca^{2+} influx and higher cytosolic Ca^{2+} levels in hADSC cells after thermal cycles decrease YAP nuclear localization (activity) (Deng et al., 2020). Given the role of TRP channels in the thermal-induced changes in Ca^{2+} influx, we simulated the experiment by cyclic activation of the TRP channel in the model with a similar temperature cycle reported for hADSC cells (Deng et al., 2020). The model predicts a cyclic response for YAP/TAZ with a range of activities lower than its initial.

In a study by Franklin et al. (2020), authors showed a rapid YAP localization reset after Tg stimulation, including an initial fast depletion of nuclear YAP followed by slow nuclear enrichment on the time scale of 0.5–2h with a steady-state YAP/TAZ N/C mean value lower than its initial. As shown in Fig. 4A, the model predicts similar YAP localization reset in around 2 hours leading to a decreased steady-state YAP/TAZ N/C. While steady-state YAP N/C is reduced in both experiment and model, authors indicated higher expression of YAP target genes after Tg stimulation and linked higher gene expression to the reentry of YAP to the nucleus. This observation highlights the significance of YAP/TAZ temporal dynamics in regulating cellular functions. Thus, part of the reported diversity in the Ca^{2+}-YAP/TAZ relationship may originate from differences between studies in measuring YAP/TAZ activity based on changes in the steady-state YAP/TAZ N/C or expression of YAP/TAZ target genes.

In another study, Pathak et al. (2014) found that ECM stiffness-induced Ca^{2+} influx by Piezo1 is required for Y AP nuclear localization when human neural stem cells (hNSPCs) grow on a stiff surface. They observed that hNSPCs transfected with Piezo1 siRNA displayed nuclear exclusion more frequently than cells transfected with non-targeting siRNA when grown on glass coverslips (Pathak et al., 2014). To reproduce the experiment conditions, we simulated YAP/TAZ N/C after ECM stiffness stimulus (glass~ 70 GPa range) with and without TRP channel knockdown. In the model, the TRP channel is responsible for sensing ECM stiffness-induced changes in cytosolic Ca^{2+}, similar to the observed Piezo1 function in hNSPCs. Consistent with the experiment, the model predicts a significant

reduction in ECM stiffness-induced YAP/TAZ N/C increase after the knockdown of the TRP channel. Finally, Wang et al. (2020) displayed that Ca^{2+} ionophore ionomycin increases TAZ in human hepatocytes. We simulated this experiment by reproducing iono-induced Ca^{2+} transient (Morgan & Jacob, 1994; Gil-Parrado et al., 2002) via a short-time (30 s) increase in Ca^{2+} influx through the plasma membrane (doubling Kf_{PM} parameter; see Table 2), which results in a Ca^{2+} transient similar to Ang II-induced Ca^{2+} (Fig. 4A). The model predicts an increase in RhoA (2h) and TAZ activities (4h and later) after ionomycin agreeing with the experimental observations.

4.4 Future directions

In our model, although we calibrated the model to capture ECM stiffness-induced cell response to simulate experiment conditions, fully understanding the impact of concurrent biochemical and biomechanical stimuli on the Ca^{2+}-YAP/TAZ relationship requires more time-course data and spatial modeling (Sun et al., 2017). Moreover, the varied 3D geometry of cells could also be one of the factors leading to the divergent Ca^{2+}-YAP/TAZ relationship. As discussed in Scott et al. study (Scott et al., 2021), three-dimensional (3D) environments made the YAP/TAZ activation by stiffness uncertain. Thus, a computational model considering both temporal and spatial dynamics of YAP/TAZ regulations is desired to predict the impacts of concurrent stimuli as well as cell geometry on the Ca^{2+}-YAP/TAZ relationship. Accordingly, in a future study, we aim to provide a comprehensive model of YAP/TAZ capturing both temporal and spatial dynamics of Ca^{2+}-mediated YAP/TAZ activation.

Summary

Experimental findings suggest that Ca^{2+} could be an intracellular messenger for the Hippo-YAP/TAZ pathway in response to biomechanical and biochemical stimuli. However, studies reported contradictory Ca^{2+}-YAP/TAZ relationships in different cell contexts, making it difficult to unravel the role of Ca^{2+} in YAP/TAZ-dependent cellular functions from a purely experimental approach. In this study, we developed a network model of Ca^{2+}-mediated YAP/TAZ signaling and investigated underlying mechanisms regulating the Ca^{2+}-YAP/TAZ relationship, as observed in experiments. The model predicted the role of Ca^{2+} temporal dynamics, CaMKII autonomous activity, and stimulus frequency in modifying the Ca^{2+}-YAP/TAZ relationship. The model predicted Ca^{2+}-YAP/TAZ distinct relationships in different settings consistent with experiments. This model provides a coherent framework to predict the cell response to biochemical and biomechanical stimuli integrated through Ca^{2+} signaling.

Funding

This work was supported in part by the Wu Tsai Human Performance Alliance at UCSD to SIF and PR. AK was also supported by an AHA postdoctoral fellowship (ID: 898850).

Data availability statement

All data generated or analyzed during this study are included in this published article. The model's MATLAB code, including model species, parameters, reaction rates, and systems of ODEs, is available at https://github.com/mkm1712/Calcium_YAP-TAZ.

List of Abbreviations

AKT	Protein kinase B
Ang II	Angiotensin II
Arp2/3	Actin-related protein 2/3 complex
CaMKII	Calcium/calmodulin-dependent protein kinase II
DAG	Diacylglycerol
ECM	Extracellular matrix
ER	Endoplasmic reticulum
FAK	Focal adhesion kinase
GPCRs	G-protein coupled receptors
IP_3	Inositol 1,4,5-trisphosphate
IP_3R	IP_3 receptor
JNK	c-Jun N-terminal kinase
LATS1/2	Large tumor suppressors 1 and 2
LIMK	LIM kinase
mDia	Mammalian diaphanous-related formin
Merlin	Moesin-ezrin-radixin like
MST1/2	Mammalian STE20-like protein kinase 1/2
Myo	Myosin light chain
NPCs	Nuclear pore complexes
PA	Phosphatidic acid
PIP2	Phosphatidylinositol 4,5-bisphosphate
PKC	Protein kinase C
PLCβ	Phospholipase C β
PLD	Phospholipase D

PMCA	Plasma membrane Ca^{2+} ATPase
PP2A	Protein Phosphatase 2A
Pyk2	Protein tyrosine kinase 2
RhoA	Rho family of GTPases
ROCK	Rho-associated kinase
RyRs	Ryanodine receptors
SERCA	Sarco/endoplasmic reticulum Ca2+-ATPase
SOCE	Store-operated calcium entry
TAZ	Transcriptional coactivator with PDZ-binding motif
TEADs	TEA domain transcription factors
Tg	Thapsigargin
TPC2	Two-pore channel 2
TRPV4	Transient receptor potential vanilloid-type 4
YAP	Yes-associated protein

References

Abdellatif MM, Neubauer CF, Lederer WJ & Rogers TB (1991). Angiotensin-induced desensitization of the phosphoinositide pathway in cardiac cells occurs at the level of the receptor. Circ Res 69, 800–809. [PubMed: 1651818]

Archibald A, Al-Masri M, Liew-Spilger A & McCaffrey L (2015). Atypical protein kinase C induces cell transformation by disrupting Hippo/Yap signaling. Mol Biol Cell 26, 3578–3595. [PubMed: 26269582]

Artemenko Y, Axiotakis L Jr, Borleis J, Iglesias PA & Devreotes PN (2016). Chemical and mechanical stimuli act on common signal transduction and cytoskeletal networks. Proc Natl Acad Sci U S A 113, E7500–E7509. [PubMed: 27821730]

Azeloglu EU & Iyengar R (2015). Signaling networks: information flow, computation, and decision making. Cold Spring Harb Perspect Biol 7, a005934. [PubMed: 25833842]

Bae SJ & Luo X (2018). Activation mechanisms of the Hippo kinase signaling cascade. Biosci Rep; DOI: 10.1042/BSR20171469.

Baker HL, Errington RJ, Davies SC & Campbell AK (2002). A Mathematical Model Predicts that Calreticulin Interacts with the Endoplasmic Reticulum Ca2+-ATPase. Biophys J 82, 582–590. [PubMed: 11806903]

Balesdent M, Brevaul L, Lacaze S, Missoum S & Morio J (2016). 8 - Methods for high-dimensional and computationally intensive models. In Estimation of Rare Event Probabilities in Complex Aerospace and Other Systems, ed. Morio J & Balesdent M, pp. 109–136. Woodhead Publishing.

Barra Avila D, Melendez-Alvarez JR & Tian X-J (2021). Control of tissue homeostasis, tumorigenesis, and degeneration by coupled bidirectional bistable switches. PLoS Comput Biol 17, e1009606. [PubMed: 34797839]

Barreto S, Gonzalez-Vazquez A, Cameron AR, Cavanagh B, Murray DJ & O'Brien FJ (2017). Identification of the mechanisms by which age alters the mechanosensitivity of mesenchymal

stromal cells on substrates of differing stiffness: Implications for osteogenesis and angiogenesis. Acta Biomater 53, 59–69. [PubMed: 28216301]

Beamish JA, Chen E & Putnam AJ (2017). Engineered extracellular matrices with controlled mechanics modulate renal proximal tubular cell epithelialization. PLoS One 12, e0181085. [PubMed: 28715434]

Bhalla US & Iyengar R (1999). Emergent properties of networks of biological signaling pathways. Science 283, 381–387. [PubMed: 9888852]

Bollag WB, Barrett PQ, Isales CM & Rasmussen H (1991). Angiotensin-II-induced changes in diacylglycerol levels and their potential role in modulating the steroidogenic response. Endocrinology 128, 231–241. [PubMed: 1702701]

Bouallegue A, Simo Cheyou ER, Anand-Srivastava MB & Srivastava AK (2013). ET-1-induced growth promoting responses involving ERK1/2 and PKB signaling and Egr-1 expression are mediated by Ca2+/CaM-dependent protein kinase-II in vascular smooth muscle cells. Cell Calcium 54, 428–435. [PubMed: 24238620]

Buxboim A, Swift J, Irianto J, Spinler KR, Dingal PCDP, Athirasala A, Kao Y-RC, Cho S, Harada T, Shin J-W & Discher DE (2014). Matrix elasticity regulates lamin-A,C phosphorylation and turnover with feedback to actomyosin. Curr Biol 24, 1909–1917. [PubMed: 25127216]

Byrd RH, Gilbert JC & Nocedal J (2000). A trust region method based on interior point techniques for nonlinear programming. Theory Decis Libr Ser C Game Theory Math Program Oper Res 89, 149–185.

Cai X, Wang K-C & Meng Z (2021). Mechanoregulation of YAP and TAZ in Cellular Homeostasis and Disease Progression. Front Cell Dev Biol 9, 673599. [PubMed: 34109179]

Caliari SR, Vega SL, Kwon M, Soulas EM & Burdick JA (2016). Dimensionality and spreading influence MSC YAP/TAZ signaling in hydrogel environments. Biomaterials 103, 314–323. [PubMed: 27429252]

Cao L, Kerleau M, Suzuki EL, Wioland H, Jouet S, Guichard B, Lenz M, Romet-Lemonne G & Jegou A (2018). Modulation of formin processivity by profilin and mechanical tension. Elife; DOI: 10.7554/elife.34176.

Codelia VA, Sun G & Irvine KD (2014). Regulation of YAP by mechanical strain through Jnk and Hippo signaling. Curr Biol 24, 2012–2017. [PubMed: 25127217]

Cooling M, Hunter P & Crampin EJ (2007). Modeling hypertrophic IP3 transients in the cardiac myocyte. Biophys J 93, 3421–3433. [PubMed: 17693463]

D'Amore A, Hanbashi AA, Di Agostino S, Palombi F, Sacconi A, Voruganti A, Taggi M, Canipari R, Blandino G, Parrington J & Filippini A (2020). Loss of Two-Pore Channel 2 (TPC2) Expression Increases the Metastatic Traits of Melanoma Cells by a Mechanism Involving the Hippo Signalling Pathway and Store-Operated Calcium Entry. Cancers ; DOI: 10.3390/cancers12092391.

Dang DK, Makena MR, Llongueras JP, Prasad H, Ko M, Bandral M & Rao R (2019). A Ca2+-ATPase Regulates E-cadherin Biogenesis and Epithelial-Mesenchymal Transition in Breast Cancer Cells. Mol Cancer Res 17, 1735–1747. [PubMed: 31076498]

Das A, Fischer RS, Pan D & Waterman CM (2016). YAP Nuclear Localization in the Absence of Cell-Cell Contact Is Mediated by a Filamentous Actin-dependent, Myosin II- and Phospho-YAP-independent Pathway during Extracellular Matrix Mechanosensing. J Biol Chem 291, 6096–6110. [PubMed: 26757814]

Dasgupta I & McCollum D (2019). Control of cellular responses to mechanical cues through YAP/TAZ regulation. J Biol Chem 294, 17693–17706. [PubMed: 31594864]

De Young GW & Keizer J (1992). A single-pool inositol 1,4,5-trisphosphate-receptor-based model for agonist-stimulated oscillations in Ca2+ concentration. Proc Natl Acad Sci U S A 89, 9895–9899. [PubMed: 1329108]

Deng Z, Wang W, Xu X, Gould OEC, Kratz K, Ma N & Lendlein A (2020). Polymeric sheet actuators with programmable bioinstructivity. Proc Natl Acad Sci U S A 117, 1895–1901. [PubMed: 31932451]

Dolan AT & Diamond SL (2014). Systems Modeling of Ca2+ Homeostasis and Mobilization in Platelets Mediated by IP3 and Store-Operated Ca2+ Entry. Biophys J 106, 2049–2060. [PubMed: 24806937]

Dolgacheva LP, Turovskaya MV, Dynnik VV, Zinchenko VP, Goncharov NV, Davletov B & Turovsky EA (2016). Angiotensin II activates different calcium signaling pathways in adipocytes. Arch Biochem Biophys 593, 38–49. [PubMed: 26850364]

Dupont G, Falcke M, Kirk V & Sneyd J (2016). Models of Calcium Signalling. Springer International Publishing.

Dupont S, Morsut L, Aragona M, Enzo E, Giulitti S, Cordenonsi M, Zanconato F, Le Digabel J, Forcato M, Bicciato S, Elvassore N & Piccolo S (2011). Role of YAP/TAZ in mechanotransduction. Nature 474, 179–183. [PubMed: 21654799]

Elosegui-Artola A, Andreu I, Beedle AEM, Lezamiz A, Uroz M, Kosmalska AJ, Oria R, Kechagia JZ, Rico-Lastres P, Le Roux A-L, Shanahan CM, Trepat X, Navajas D, Garcia-Manyes S & Roca-Cusachs P (2017). Force Triggers YAP Nuclear Entry by Regulating Transport across Nuclear Pores. Cell 171, 1397–1410.e14. [PubMed: 29107331]

Franklin JM, Ghosh RP, Shi Q, Reddick MP & Liphardt JT (2020). Concerted localization-resets precede YAP-dependent transcription. Nat Commun 11, 4581. [PubMed: 32917893]

Furth N, Pateras IS, Rotkopf R, Vlachou V, Rivkin I, Schmitt I, Bakaev D, Gershoni A, Ainbinder E, Leshkowitz D, Johnson RL, Gorgoulis VG, Oren M & Aylon Y (2018). LATS1 and LATS2 suppress breast cancer progression by maintaining cell identity and metabolic state. Life Sci Alliance 1, e201800171. [PubMed: 30456386]

Galan JA & Avruch J (2016). MST1/MST2 Protein Kinases: Regulation and Physiologic Roles. Biochemistry 55, 5507–5519. [PubMed: 27618557]

Gil-Parrado S, Fernández-Montalván A, Assfalg-Machleidt I, Popp O, Bestvater F, Holloschi A, Knoch TA, Auerswald EA, Welsh K, Reed JC, Fritz H, Fuentes-Prior P, Spiess E, Salvesen GS & Machleidt W (2002). Ionomycin-activated calpain triggers apoptosis. A probable role for Bcl-2 family members. J Biol Chem 277, 27217–27226. [PubMed: 12000759]

Gong R, Hong AW, Plouffe SW, Zhao B, Liu G, Yu F-X, Xu Y & Guan K-L (2015). Opposing roles of conventional and novel PKC isoforms in Hippo-YAP pathway regulation. Cell Res 25, 985–988. [PubMed: 26206313]

Gordge PC, Hulme MJ, Clegg RA & Miller WR (1996). Elevation of protein kinase A and protein kinase C activities in malignant as compared with normal human breast tissue. Eur J Cancer 32A, 2120–2126. [PubMed: 9014755]

Gudlur A, Zeraik AE, Hirve N, Rajanikanth V, Bobkov AA, Ma G, Zheng S, Wang Y, Zhou Y, Komives EA & Hogan PG (2018). Calcium sensing by the STIM1 ER-luminal domain. Nat Commun 9, 4536. [PubMed: 30382093]

Guo X & Zhao B (2013). Integration of mechanical and chemical signals by YAP and TAZ transcription coactivators. Cell Biosci 3, 33. [PubMed: 23985334]

Han S, Pang M-F & Nelson CM (2018). Substratum stiffness tunes proliferation downstream of Wnt3a in part by regulating integrin-linked kinase and frizzled-1. J Cell Sci; DOI: 10.1242/jcs.210476.

Hao Y, Chun A, Cheung K, Rashidi B & Yang X (2008). Tumor suppressor LATS1 is a negative regulator of oncogene YAP. J Biol Chem 283, 5496–5509. [PubMed: 18158288]

Harootunian AT, Kao JP, Paranjape S & Tsien RY (1991). Generation of calcium oscillations in fibroblasts by positive feedback between calcium and IP3. Science 251, 75–78. [PubMed: 1986413]

Haws HJ, McNeil MA & Hansen MDH (2016). Control of cell mechanics by RhoA and calcium fluxes during epithelial scattering. Tissue Barriers 4, e1187326. [PubMed: 27583192]

Hein AL, Brandquist ND, Ouellette CY, Seshacharyulu P, Enke CA, Ouellette MM, Batra SK & Yan Y (2019). PR55α regulatory subunit of PP2A inhibits the MOB1/LATS cascade and activates YAP in pancreatic cancer cells. Oncogenesis 8, 63. [PubMed: 31659153]

Hom JR, Gewandter JS, Michael L, Sheu S-S & Yoon Y (2007). Thapsigargin induces biphasic fragmentation of mitochondria through calcium-mediated mitochondrial fission and apoptosis. J Cell Physiol 212, 498–508. [PubMed: 17443673]

Hong W & Guan K-L (2012). The YAP and TAZ transcription co-activators: key downstream effectors of the mammalian Hippo pathway. Semin Cell Dev Biol 23, 785–793. [PubMed: 22659496]

Huang XC, Richards EM & Sumners C (1995). Angiotensin II type 2 receptor-mediated stimulation of protein phosphatase 2A in rat hypothalamic/brainstem neuronal cocultures. J Neurochem 65, 2131–2137. [PubMed: 7595499]

Huang Y-W, Chang S-J, Harn HI-C, Huang H-T, Lin H-H, Shen M-R, Tang M-J & Chiu W-T (2015). Mechanosensitive store-operated calcium entry regulates the formation of cell polarity. J Cell Physiol 230, 2086–2097. [PubMed: 25639747]

Iribe G, Kohl P & Noble D (2006). Modulatory effect of calmodulin-dependent kinase II (CaMKII) on sarcoplasmic reticulum Ca2+ handling and interval-force relations: a modelling study. Philos Trans A Math Phys Eng Sci 364, 1107–1133. [PubMed: 16608699]

Jang J-W, Kim M-K & Bae S-C (2020). Reciprocal regulation of YAP/TAZ by the Hippo pathway and the Small GTPase pathway. Small GTPases 11, 280–288. [PubMed: 29457552]

Janmey PA, Fletcher DA & Reinhart-King CA (2020). Stiffness Sensing by Cells. Physiol Rev 100, 695–724. [PubMed: 31751165]

Jiang Y, Zhang H, Wang J, Liu Y, Luo T & Hua H (2022). Targeting extracellular matrix stiffness and mechanotransducers to improve cancer therapy. J Hematol Oncol 15, 34. [PubMed: 35331296]

Kang M & Othmer HG (2007). The variety of cytosolic calcium responses and possible roles of PLC and PKC. Phys Biol 4, 325–343. [PubMed: 18185010]

Khalilimeybodi A, Daneshmehr A & Sharif Kashani B (2018). Ca2+-dependent calcineurin/NFAT signaling in β-adrenergic-induced cardiac hypertrophy. Gen Physiol Biophys 37, 41–56. [PubMed: 29424351]

Khalilimeybodi A, Paap AM, Christiansen SLM & Saucerman JJ (2020). Context-specific network modeling identifies new crosstalk in β-adrenergic cardiac hypertrophy. PLoS Comput Biol 16, e1008490. [PubMed: 33338038]

Khalilimeybodi A, Riaz M, Campbell SG, Omens JH, McCulloch AD, Qyang Y, Saucerman JJ (2022). Signaling network model of cardiomyocyte morphological changes in familial cardiomyopathy. J Mol Cell Cardiol.

Khare YP, Muñoz-Carpena R, Rooney RW & Martinez CJ (2015). A multi-criteria trajectory-based parameter sampling strategy for the screening method of elementary effects. Environmental Modelling & Software 64, 230–239.

Kholodenko BN (2006). Cell-signalling dynamics in time and space. Nat Rev Mol Cell Biol 7, 165–176. [PubMed: 16482094]

Kline D & Kline JT (1992). Thapsigargin activates a calcium influx pathway in the unfertilized mouse egg and suppresses repetitive calcium transients in the fertilized egg. J Biol Chem 267, 17624–17630. [PubMed: 1387638]

Kodaka M & Hata Y (2015). The mammalian Hippo pathway: regulation and function of YAP1 and TAZ. Cell Mol Life Sci 72, 285–306. [PubMed: 25266986]

Kolahi KS & Mofrad MRK (2010). Mechanotransduction: a major regulator of homeostasis and development. Wiley Interdiscip Rev Syst Biol Med 2, 625–639. [PubMed: 20890961]

Kowalewski JM, Uhlén P, Kitano H & Brismar H (2006). Modeling the impact of store-operated Ca2+ entry on intracellular Ca2+ oscillations. Math Biosci 204, 232–249. [PubMed: 16620876]

Kushida N, Kabuyama Y, Yamaguchi O & Homma Y (2001). Essential role for extracellular Ca2+ in JNK activation by mechanical stretch in bladder smooth muscle cells. Am J Physiol Cell Physiol 281, C1165–C1172. [PubMed: 11546652]

Lampi MC, Faber CJ, Huynh J, Bordeleau F, Zanotelli MR & Reinhart-King CA (2016). Simvastatin Ameliorates Matrix Stiffness-Mediated Endothelial Monolayer Disruption. PLoS One 11, e0147033. [PubMed: 26761203]

Lauffenburger DA (2000). Cell signaling pathways as control modules: complexity for simplicity? Proc Natl Acad Sci U S A 97, 5031–5033. [PubMed: 10805765]

Lee J-H, Kim T-S, Yang T-H, Koo B-K, Oh S-P, Lee K-P, Oh H-J, Lee S-H, Kong Y-Y, Kim J-M & Lim D-S (2008). A crucial role of WW45 in developing epithelial tissues in the mouse. EMBO J 27, 1231–1242. [PubMed: 18369314]

Lee JY, Chang JK, Dominguez AA, Lee H-P, Nam S, Chang J, Varma S, Qi LS, West RB & Chaudhuri O (2019). YAP-independent mechanotransduction drives breast cancer progression. Nat Commun 10, 1848. [PubMed: 31015465]

Legewie S, Herzel H, Westerhoff HV & Blüthgen N (2008). Recurrent design patterns in the feedback regulation of the mammalian signalling network. Mol Syst Biol 4, 190. [PubMed: 18463614]

Lessey EC, Guilluy C & Burridge K (2012). From mechanical force to RhoA activation. Biochemistry 51, 7420–7432. [PubMed: 22931484]

Li F & Malik KU (2005). Angiotensin II-induced Akt activation is mediated by metabolites of arachidonic acid generated by CaMKII-stimulated Ca2(+)-dependent phospholipase A2. Am J Physiol Heart Circ Physiol 288, H2306–16. [PubMed: 15637121]

Li L, Ren CH, Tahir SA, Ren C & Thompson TC (2003). Caveolin-1 maintains activated Akt in prostate cancer cells through scaffolding domain binding site interactions with and inhibition of serine/threonine protein phosphatases PP1 and PP2A. Mol Cell Biol 23, 9389–9404. [PubMed: 14645548]

Liu Z, Wei Y, Zhang L, Yee PP, Johnson M, Zhang X, Gulley M, Atkinson JM, Trebak M, Wang H-G & Li W (2019). Induction of store-operated calcium entry (SOCE) suppresses glioblastoma growth by inhibiting the Hippo pathway transcriptional coactivators YAP/TAZ. Oncogene 38, 120–139. [PubMed: 30082911]

Lomakin A, Nader G & Piel M (2017). Forcing Entry into the Nucleus. Dev Cell 43, 547–548. [PubMed: 29207257]

Low BC, Pan CQ, Shivashankar GV, Bershadsky A, Sudol M & Sheetz M (2014). YAP/TAZ as mechanosensors and mechanotransducers in regulating organ size and tumor growth. FEBS Lett 588, 2663–2670. [PubMed: 24747426]

Luik RM, Wang B, Prakriya M, Wu MM & Lewis RS (2008). Oligomerization of STIM1 couples ER calcium depletion to CRAC channel activation. Nature 454, 538–542. [PubMed: 18596693]

Lukas TJ (2004). A signal transduction pathway model prototype I: From agonist to cellular endpoint. Biophys J 87, 1406–1416. [PubMed: 15345523]

Ma S, Meng Z, Chen R & Guan K-L (2019). The Hippo Pathway: Biology and Pathophysiology. Annu Rev Biochem 88, 577–604. [PubMed: 30566373]

Mammoto A, Huang S, Moore K, Oh P & Ingber DE (2004). Role of RhoA, mDia, and ROCK in cell shape-dependent control of the Skp2-p27kip1 pathway and the G1/S transition. J Biol Chem 279, 26323–26330. [PubMed: 15096506]

Maurya MR & Subramaniam S (2007). A kinetic model for calcium dynamics in RAW 264.7 cells: 1. Mechanisms, parameters, and subpopulational variability. Biophys J 93, 709–728. [PubMed: 17483174]

Meng Z, Moroishi T & Guan K-L (2016). Mechanisms of Hippo pathway regulation. Genes Dev 30, 1–17. [PubMed: 26728553]

Michalski PJ (2013). The delicate bistability of CaMKII. Biophys J 105, 794–806. [PubMed: 23931327]

Miller CJ & Davidson LA (2013). The interplay between cell signalling and mechanics in developmental processes. Nat Rev Genet 14, 733–744. [PubMed: 24045690]

Moraru II, Schaff JC, Slepchenko BM, Blinov ML, Morgan F, Lakshminarayana A, Gao F, Li Y & Loew LM (2008). Virtual Cell modelling and simulation software environment. IET Syst Biol 2, 352–362. [PubMed: 19045830]

Morgan AJ & Jacob R (1994). Ionomycin enhances Ca2+ influx by stimulating store-regulated cation entry and not by a direct action at the plasma membrane. Biochem J 300 (Pt 3), 665–672. [PubMed: 8010948]

Moroishi T, Park HW, Qin B, Chen Q, Meng Z, Plouffe SW, Taniguchi K, Yu F-X, Karin M, Pan D & Guan K-L (2015). A YAP/TAZ-induced feedback mechanism regulates Hippo pathway homeostasis. Genes Dev 29, 1271–1284. [PubMed: 26109050]

Mukherjee R, Vanaja KG, Boyer JA, Gadal S, Solomon H, Chandarlapaty S, Levchenko A & Rosen N (2021). Regulation of PTEN translation by PI3K signaling maintains pathway homeostasis. Mol Cell 81, 708–723.e5. [PubMed: 33606974]

Naito T, Masaki T, Nikolic-Paterson DJ, Tanji C, Yorioka N & Kohno N (2004). Angiotensin II induces thrombospondin-1 production in human mesangial cells via p38 MAPK and JNK: a mechanism for activation of latent TGF-beta1. Am J Physiol Renal Physiol 286, F278–87. [PubMed: 14583433]

Palazzo AF, Eng CH, Schlaepfer DD, Marcantonio EE & Gundersen GG (2004). Localized stabilization of microtubules by integrin- and FAK-facilitated Rho signaling. Science 303, 836–839. [PubMed: 14764879]

Pathak MM, Nourse JL, Tran T, Hwe J, Arulmoli J, Le DTT, Bernardis E, Flanagan LA & Tombola F (2014). Stretch-activated ion channel Piezo1 directs lineage choice in human neural stem cells. Proc Natl Acad Sci U S A 111, 16148–16153. [PubMed: 25349416]

Pi HJ & Lisman JE (2008). Coupled phosphatase and kinase switches produce the tristability required for long-term potentiation and long-term depression. J Neurosci 28, 13132–13138. [PubMed: 19052204]

Piccolo S, Dupont S & Cordenonsi M (2014). The biology of YAP/TAZ: hippo signaling and beyond. Physiol Rev 94, 1287–1312. [PubMed: 25287865]

Pocaterra A, Romani P & Dupont S (2020). YAP/TAZ functions and their regulation at a glance. J Cell Sci; DOI: 10.1242/jcs.230425.

Poli R, Kennedy J & Blackwell T (2007). Particle swarm optimization. Swarm Intelligence 1, 33–57.

Pollard TD, Blanchoin L & Mullins RD (2000). Molecular mechanisms controlling actin filament dynamics in nonmuscle cells. Annu Rev Biophys Biomol Struct 29, 545–576. [PubMed: 10940259]

Praskova M, Khoklatchev A, Ortiz-Vega S & Avruch J (2004). Regulation of the MST1 kinase by autophosphorylation, by the growth inhibitory proteins, RASSF1 and NORE1, and by Ras. Biochem J 381, 453–462. [PubMed: 15109305]

Rangamani P, Levy MG, Khan S & Oster G (2016). Paradoxical signaling regulates structural plasticity in dendritic spines. Proc Natl Acad Sci U S A 113, E5298–307. [PubMed: 27551076]

Rodriguez ML, Beussman KM, Chun KS, Walzer MS, Yang X, Murry CE & Sniadecki NJ (2019). Substrate Stiffness, Cell Anisotropy, and Cell-Cell Contact Contribute to Enhanced Structural and Calcium Handling Properties of Human Embryonic Stem Cell-Derived Cardiomyocytes. ACS Biomater Sci Eng 5, 3876–3888. [PubMed: 33438427]

Romano D, Nguyen LK, Matallanas D, Halasz M, Doherty C, Kholodenko BN & Kolch W (2014). Protein interaction switches coordinate Raf-1 and MST2/Hippo signalling. Nat Cell Biol 16, 673–684. [PubMed: 24929361]

Sabri A, Govindarajan G, Griffin TM, Byron KL, Samarel AM & Lucchesi PA (1998). Calcium- and protein kinase C-dependent activation of the tyrosine kinase PYK2 by angiotensin II in vascular smooth muscle. Circ Res 83, 841–851. [PubMed: 9776731]

Sadoshima J & Izumo S (1993). Signal transduction pathways of angiotensin II--induced c-fos gene expression in cardiac myocytes in vitro. Roles of phospholipid-derived second messengers. Circ Res 73, 424–438. [PubMed: 8348687]

Scott KE, Fraley SI & Rangamani P (2021). A spatial model of YAP/TAZ signaling reveals how stiffness, dimensionality, and shape contribute to emergent outcomes. Proc Natl Acad Sci U S A; DOI: 10.1073/pnas.2021571118.

Scott KE, Rychel K, Ranamukhaarachchi S, Rangamani P & Fraley SI (2019). Emerging themes and unifying concepts underlying cell behavior regulation by the pericellular space. Acta Biomater 96, 81–98. [PubMed: 31176842]

Seshacharyulu P, Pandey P, Datta K & Batra SK (2013). Phosphatase: PP2A structural importance, regulation and its aberrant expression in cancer. Cancer Lett 335, 9–18. [PubMed: 23454242]

Sharma S, Goswami R, Merth M, Cohen J, Lei KY, Zhang DX & Rahaman SO (2017). TRPV4 ion channel is a novel regulator of dermal myofibroblast differentiation. Am J Physiol Cell Physiol 312, C562–C572. [PubMed: 28249987]

Shin S-Y & Nguyen LK (2016). Unveiling Hidden Dynamics of Hippo Signalling: A Systems Analysis. Genes ; DOI: 10.3390/genes7080044.

Solon J, Levental I, Sengupta K, Georges PC & Janmey PA (2007). Fibroblast adaptation and stiffness matching to soft elastic substrates. Biophys J 93, 4453–4461. [PubMed: 18045965]

Spiering D & Hodgson L (2011). Dynamics of the Rho-family small GTPases in actin regulation and motility. Cell Adh Migr 5, 170–180. [PubMed: 21178402]

Sun M, Chi G, Xu J, Tan Y, Xu J, Lv S, Xu Z, Xia Y, Li L & Li Y (2018). Extracellular matrix stiffness controls osteogenic differentiation of mesenchymal stem cells mediated by integrin α5. Stem Cell Res Ther 9, 52. [PubMed: 29490668]

Sun M, Spill F & Zaman MH (2016). A Computational Model of YAP/TAZ Mechanosensing. Biophys J 110, 2540–2550. [PubMed: 27276271]

Sun Y, Deng R, Zhang K, Ren X, Zhang L & Li J (2017). Single-cell study of the extracellular matrix effect on cell growth by in situ imaging of gene expression. Chem Sci 8, 8019–8024. [PubMed: 29568449]

Swift J, Ivanovska IL, Buxboim A, Harada T, Dingal PCDP, Pinter J, Pajerowski JD, Spinler KR, Shin J-W, Tewari M, Rehfeldt F, Speicher DW & Discher DE (2013). Nuclear lamin-A scales with tissue stiffness and enhances matrix-directed differentiation. Science 341, 1240104. [PubMed: 23990565]

Tajada S & Villalobos C (2020). Calcium Permeable Channels in Cancer Hallmarks. Front Pharmacol 11, 968. [PubMed: 32733237]

Timmins JM, Ozcan L, Seimon TA, Li G, Malagelada C, Backs J, Backs T, Bassel-Duby R, Olson EN, Anderson ME & Tabas I (2009). Calcium/calmodulin-dependent protein kinase II links ER stress with Fas and mitochondrial apoptosis pathways. J Clin Invest 119, 2925–2941. [PubMed: 19741297]

Totaro A, Panciera T & Piccolo S (2018). YAP/TAZ upstream signals and downstream responses. Nat Cell Biol 20, 888–899. [PubMed: 30050119]

Urtreger AJ, Kazanietz MG & Bal de Kier Joffé ED (2012). Contribution of individual PKC isoforms to breast cancer progression. IUBMB Life 64, 18–26. [PubMed: 22095874]

Wang X, Cai B, Yang X, Sonubi OO, Zheng Z, Ramakrishnan R, Shi H, Valenti L, Pajvani UB, Sandhu J, Infante RE, Radhakrishnan A, Covey DF, Guan K-L, Buck J, Levin LR, Tontonoz P, Schwabe RF & Tabas I (2020). Cholesterol Stabilizes TAZ in Hepatocytes to Promote Experimental Non-alcoholic Steatohepatitis. Cell Metab 31, 969–986.e7. [PubMed: 32259482]

Wang Y, Sherrard A, Zhao B, Melak M, Trautwein J, Kleinschnitz E-M, Tsopoulidis N, Fackler OT, Schwan C & Grosse R (2019a). GPCR-induced calcium transients trigger nuclear actin assembly for chromatin dynamics. Nat Commun 10, 5271. [PubMed: 31754104]

Wang Z, Sun L, Liang S, Liu Z-C, Zhao Z-Y, Yang J, Wang D & Yang D-Q (2019b). GPER stabilizes F-actin cytoskeleton and activates TAZ via PLCβ-PKC and Rho/ROCK-LIMK-Cofilin pathway. Biochem Biophys Res Commun 516, 976–982. [PubMed: 31277940]

Wei Y & Li W (2021). Calcium, an Emerging Intracellular Messenger for the Hippo Pathway Regulation. Front Cell Dev Biol 9, 694828. [PubMed: 34268313]

Wei Y, Yee PP, Liu Z, Zhang L, Guo H, Zheng H, Anderson B, Gulley M & Li W (2020). NEDD4L-mediated Merlin ubiquitination facilitates Hippo pathway activation. EMBO Rep 21, e50642. [PubMed: 33058421]

Yasuda R, Hayashi Y & Hell JW (2022). CaMKII: a central molecular organizer of synaptic plasticity, learning and memory. Nat Rev Neurosci; DOI: 10.1038/s41583-022-00624-2.

Ying Z, Giachini FRC, Tostes RC & Webb RC (2009). PYK2/PDZ-RhoGEF links Ca2+ signaling to RhoA. Arterioscler Thromb Vasc Biol 29, 1657–1663. [PubMed: 19759375]

Yu F-X, Zhao B, Panupinthu N, Jewell JL, Lian I, Wang LH, Zhao J, Yuan H, Tumaneng K, Li H, Fu X-D, Mills GB & Guan K-L (2012). Regulation of the Hippo-YAP pathway by G-protein-coupled receptor signaling. Cell 150, 780–791. [PubMed: 22863277]

Yu M, Yuan X, Lu C, Le S, Kawamura R, Efremov AK, Zhao Z, Kozlov MM, Sheetz M, Bershadsky A & Yan J (2017). mDia1 senses both force and torque during F-actin filament polymerization. Nat Commun 8, 1650. [PubMed: 29162803]

Zanconato F, Cordenonsi M & Piccolo S (2016). YAP/TAZ at the Roots of Cancer. Cancer Cell 29, 783–803. [PubMed: 27300434]

Zhabotinsky AM (2000). Bistability in the Ca2+/Calmodulin-Dependent Protein Kinase-Phosphatase System. Biophys J 79, 2211–2221. [PubMed: 11053103]

Zhang J, Xu Q, Ren F, Liu Y, Cai R, Yao Y & Zhou M-S (2021). Inhibition of YAP activation attenuates renal injury and fibrosis in angiotensin II hypertensive mice. Can J Physiol Pharmacol 99, 1000–1006. [PubMed: 33852804]

Health Research Alliance Author Manuscript

Zhao J-W, Gao Z-L, Ji Q-Y, Wang H, Zhang H-Y, Yang Y-D, Xing F-J, Meng L-J & Wang Y (2012). Regulation of cofilin activity by CaMKII and calcineurin. Am J Med Sci 344, 462–472. [PubMed: 22270398]

Zhong W, Chebolu S & Darmani NA (2016). Thapsigargin-induced activation of Ca(2+)-CaMKII-ERK in brainstem contributes to substance P release and induction of emesis in the least shrew. Neuropharmacology 103, 195–210. [PubMed: 26631534]

Zhou C, Ramaswamy SS, Johnson DE, Vitturi DA, Schopfer FJ, Freeman BA, Hudmon A & Levitan ES (2016). Novel Roles for Peroxynitrite in Angiotensin II and CaMKII Signaling. Sci Rep 6, 23416. [PubMed: 27079272]

Zhu W, Zou Y, Shiojima I, Kudoh S, Aikawa R, Hayashi D, Mizukami M, Toko H, Shibasaki F, Yazaki Y, Nagai R & Komuro I (2000). Ca2+/calmodulin-dependent kinase II and calcineurin play critical roles in endothelin-1-induced cardiomyocyte hypertrophy. J Biol Chem 275, 15239–15245. [PubMed: 10809760]

Health Research Alliance Author Manuscript

Key points:

- YAP/TAZ integrates biochemical and biomechanical inputs to regulate cellular functions, and Ca^{2+} acts as a key second messenger linking cellular inputs to YAP/TAZ.
- Studies reported contradictory Ca^{2+}-YAP/TAZ relationships for different cell types and stimuli.
- A network model of Ca^{2+}-mediated YAP/TAZ signaling was developed to investigate the underlying mechanisms of divergent Ca^{2+}-YAP/TAZ relationships.
- The model predicts context-dependent Ca^{2+} transient, CaMKII bistable response, and frequency-dependent activation of LATS1/2 upstream regulators as mechanisms governing the Ca^{2+}-YAP/TAZ relationship.
- This study provides new insights into the underlying mechanisms of the controversial Ca^{2+}-YAP/TAZ relationship to better understand the dynamics of cellular functions controlled by YAP/TAZ activity.

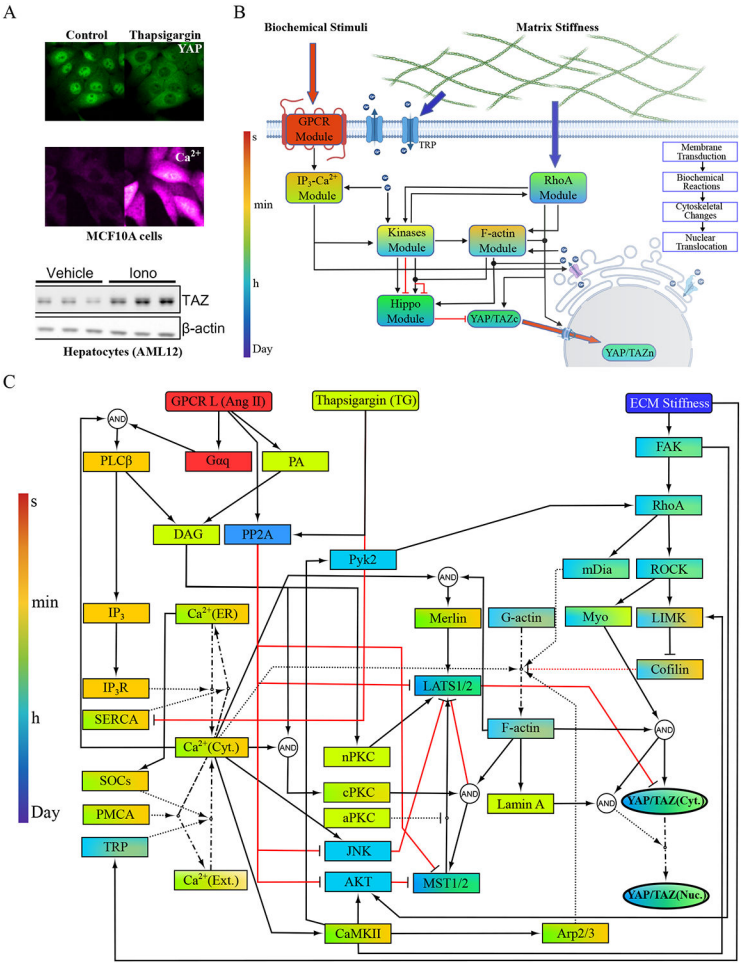

Figure 1.

A compartmental model of Ca^{2+}-mediated YAP/TAZ signaling to investigate the Ca^{2+}-YAP/TAZ context-specific relationship. (A) Divergent Ca^{2+}-YAP/TAZ relationships were observed in different experimental settings. An increase in the cytosolic Ca^{2+} level could both inhibit (MCF10A cells: adapted from (Franklin et al., 2020), which is licensed under CC by 4.0.) or activate (AML12 cells: from (Wang et al., 2020), with permission from Elsevier) YAP/TAZ. (B) Signaling modules with different dynamics (time scales) that regulate YAP/TAZ activity after biomechanical and biochemical stimuli through Ca^{2+}-mediated signaling are shown. IP_3-Ca^{2+} module links fast GPCR module activation by biochemical stimuli, particularly angiotensin II (Ang II), to intracellular Ca^{2+} in a few minutes. RhoA module mediates the regulatory effect of slow biomechanical stimuli (ECM matrix stiffness) on YAP/TAZ activity from hours to days. Cell signaling modules, including F-actin, kinases, and Hippo, contribute to Ca^{2+}-mediated YAP/TAZ regulation with various response times from minutes to hours. The time scale is shown in the color bar. Created with BioRender.com. (C) The network of signaling species and reactions connecting cell stimuli to YAP/TAZ activity. Thapsigargin (Tg), a SERCA inhibitor, is used in the model to modify intracellular Ca^{2+} directly. Activation and inhibition reactions are illustrated by black and red lines, respectively. Dot-dashed lines show species transfer between compartments. Dotted lines show species' influence on reactions.

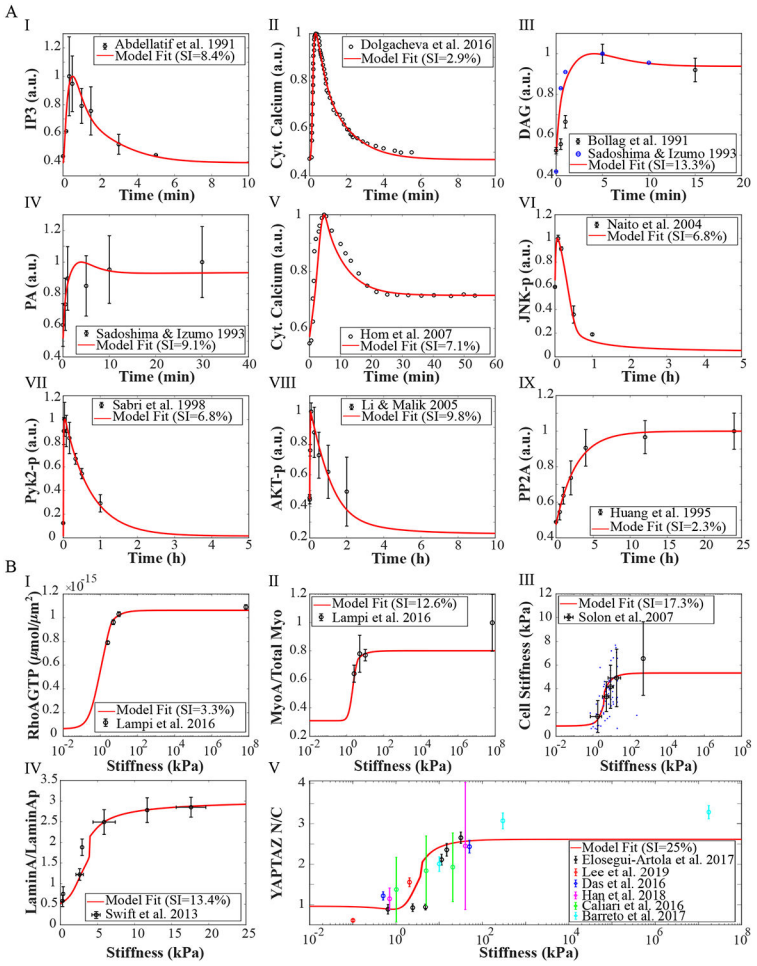

Figure 2.

The compartmental ODE model captures temporal dynamics of Ca^{2+}-mediated YAP/TAZ regulation and steady-state response of ECM stiffness-induced YAP/TAZ in the cell. The model is calibrated to time course variations of IP_3 (Abdellatif et al., 1991)(A-I), cytosolic Ca^{2+} (Dolgacheva et al., 2016) (A-II), DAG (Bollag et al., 1991; Sadoshima & Izumo, 1993) (A-III), PA (Sadoshima & Izumo, 1993) (A-IV), JNK (Naito et al., 2004) (A-VI), Pyk2 (Sabri et al., 1998) (A-VII), AKT (Li & Malik, 2005) (A-VIII), and PP2A (Huang et al., 1995) (A-IX) after Ang II (0.1μM) stimulation as well as variations of cytosolic Ca^{2+} after 1μM thapsigargin (Hom et al., 2007) (A-V). Model parameters are also estimated to capture steady-state variations of RhoA-GTP (B-I) and myosin (B-II) (Lampi et al., 2016), cell stiffness (Solon et al., 2007) (B-III), Lamin A (Swift et al., 2013) (B-IV), and the ratio of nuclear YAP/TAZ to cytosolic YAP/TAZ (Das et al., 2016; Caliari et al., 2016; Barreto et al., 2017; Elosegui-Artola et al., 2017; Han et al., 2018; Lee et al., 2019) (B-V) for a range of substrate stiffnesses.

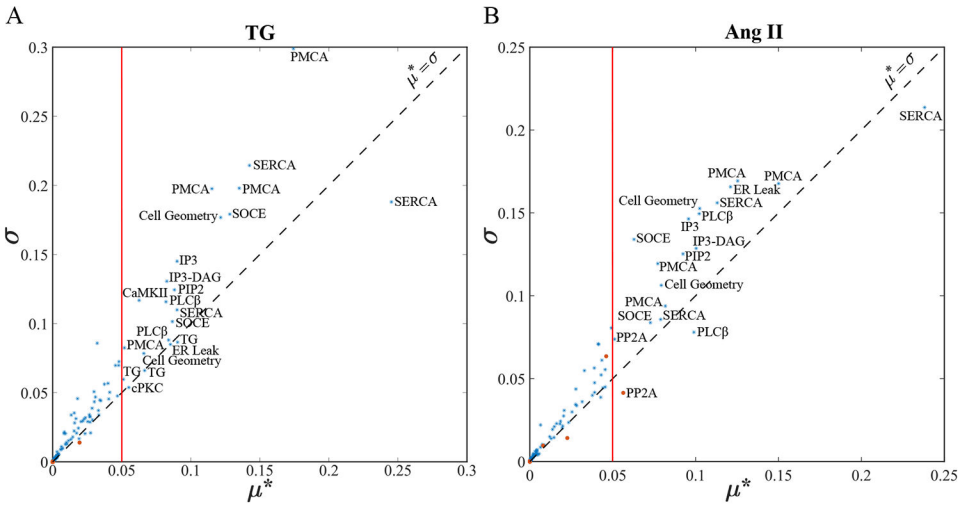

Figure 3.

Morris global sensitivity analysis reveals the main parameters of the model regulating Ca^{2+}-induced YAP/TAZ response after cell stimulation by 1 μM thapsigargin (Tg) (A) and 0.1 μM Ang II (B). Parameters with μ* > 0.05 are considered influential for Ca^{2+}-induced YAP/TAZ activity. Blue stars and orange dots indicate parameters with non-monotonic and monotonic impact on model outputs.

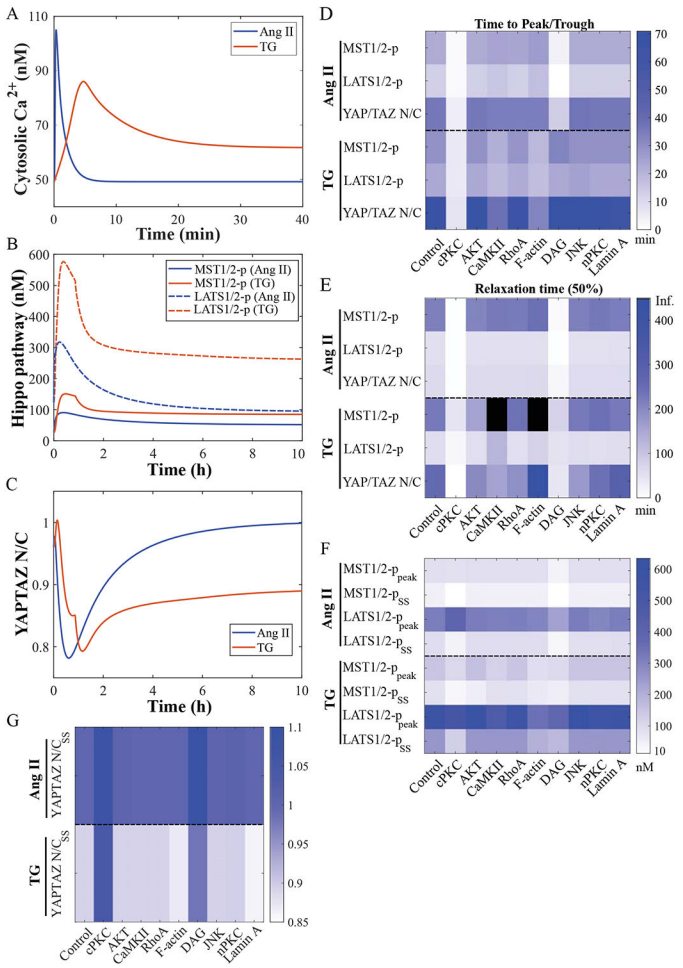

Figure 4.

The major mediators in Ca^{2+}-mediated YAP/TAZ activation. The dynamic response of Ca^{2+} (A) Hippo pathway core components (B) and YAP/TAZ activity (C) to Ang II and thapsigargin (Tg) stimuli are simulated by the model. In (D-G), the impact of knocking down each upstream regulator on temporal dynamics of Hippo-YAP/TAZ activation (D, E), steady-state and peak values of the Hippo pathway response (F), and steady-state YAP/TAZ activity (G) is shown. The impact of each upstream regulator's removal is simulated by fixing the regulator's activity to its initial condition.

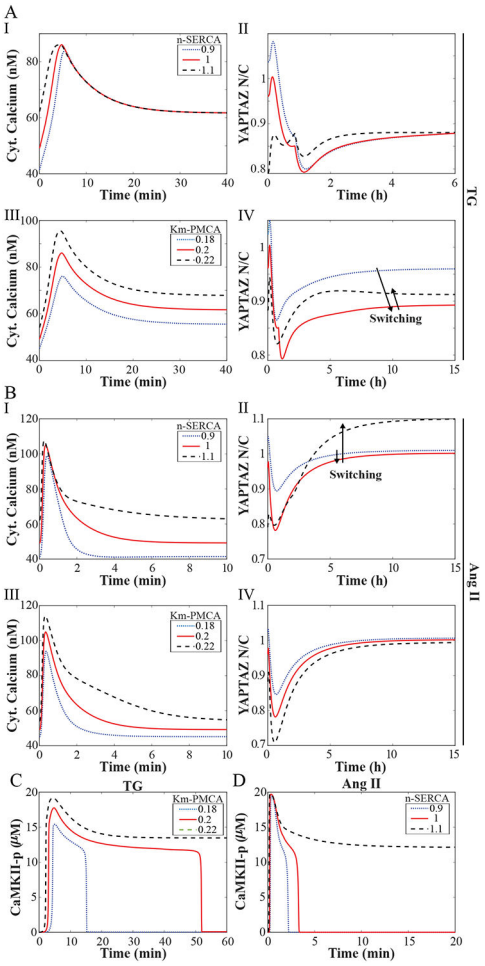

Figure 5.

Impact of Ca^{2+} dynamics on YAP/TAZ activity. (A) Time course of Ca^{2+} transient and following YAP/TAZ activity for different n-SERCA (I, II) and Km-PMCA (III, IV) values in the context of Tg stimulus. (B) Time course of Ca^{2+} transient and following YAP/TAZ activity for different n-SERCA (I, II) and Km-PMCA (III, IV) values in the context of Ang II. Black arrows indicate the direction of changes in YAP/TAZ activity based on YAP/TAZ N/C level (up/down) and shift in the trough time (right/left). (C) Bistable response of CaMKII after varying Km-PMCA in the Tg context. (D) Bistable response of CaMKII after altering n-SERCA in the Ang II context.

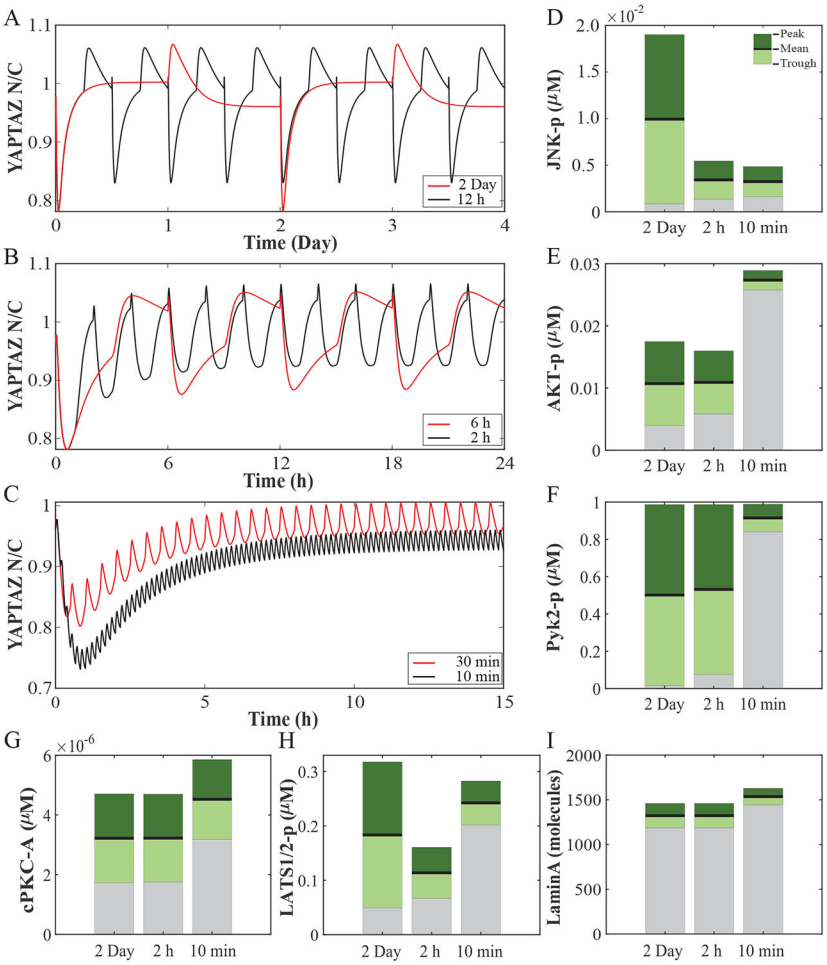

Figure 6.

The YAP/TAZ exhibits a non-monotonic response to periodic GPCR activation. (A-C) YAP/TAZ activation time course for stimulation periods from 2 Days to 10 min. The oscillation domain (green bars) and the mean activity (thick black line) of upstream regulators of YAP/TAZ, including JNK (D), AKT (E), Pyk2p (F), cPKC (G), LATS1/2 (H), and Lamin A (I) are shown for stimulation periods from 2 Day to 10 min.

Table 1

List of species in the Ca^{2+}-mediated YAP/TAZ model

Species	Guess initial level	SS initial level	Units	Ref.	Species	Guess initial level	SS initial level	Units	Ref.
GPCR Module					**RhoA Module**				
GR	2.93	2.93	$\frac{molecules}{\mu m^2}$	(Cooling et al., 2007)	FAK	1	0.7	μM	(Scott et al., 2021)
GR-GqGDP	1.07	1.07	$\frac{molecules}{\mu m^2}$	(Cooling et al., 2007)	FAK-p	0	0.3	μM	
GqGDP	10000	10000	$\frac{molecules}{\mu m^2}$	(Cooling et al., 2007)	RhoAGDP	1	0.966	μM	(Scott et al., 2021)
L-GR	0.0	0.0	$\frac{molecules}{\mu m^2}$		RhoAGTPMem.	0	37.69	$\frac{molecules}{\mu m^2}$	
L-GR-GqGDP	0.0	0.0	$\frac{molecules}{\mu m^2}$		ROCK	1	0.973	μM	(Scott et al., 2021)
L-GR-GqGDP-p	0.0	0.0	$\frac{molecules}{\mu m^2}$		ROCK*	0	0.027	μM	
GqGTP	0.0	0.0	$\frac{molecules}{\mu m^2}$		mDia	0.8	0.789	μM	(Scott et al., 2021)
IP_3- Ca^{2+} Module					mDia*	0	0.011	μM	
PLC	90.9	94.87	$\frac{molecules}{\mu m^2}$	(Cooling et al., 2007)	**F-actin Module**				
PLC- Ca^{2+}	8.63	4.66	$\frac{molecules}{\mu m^2}$	(Cooling et al., 2007)	G-actin	500	381.44	μM	(Scott et al., 2021)
PLC-GqGTP	0.0	0.0	$\frac{molecules}{\mu m^2}$		F-actin	0	118.56	μM	
PLC- Ca^{2+}-GqGTP	0.0	0.0	$\frac{molecules}{\mu m^2}$		LIMK	2	1.932	μM	(Scott et al., 2021)
PIP2	4000	4000	$\frac{molecules}{\mu m^2}$	(Cooling et al., 2007)	LIMK*	0	0.068	μM	
PA	1000	2.66	$\frac{molecules}{\mu m^2}$	A	Cofilin	2	1.82	μM	(Scott et al., 2021)
IP_3	0.0	0.014	μM		Cofilin-p	0.0	0.18	μM	
DAG	0.5	0.093	μM	A	Merlin	1	0.945	μM	
Ca^{2+}	0.095	0.049	μM	(Baker et al., 2002)	Merlin*	0.0	0.055	μM	
Ca^{2+} ER	400	267	μM	(Lukas, 2004)	Arp2/3	5	5.0	μM	(Scott et al., 2021)
Ca^{2+} ECM	950	956.2	μM	(Kowalewski et al., 2006)	Arp2/3*	0.0	0.0	μM	
Buffers	350	348.3	μM	(Lukas, 2004)	**Hippo-YAP/TAZ Module**				

Species	Guess initial level	SS initial level	Units	Ref.	Species	Guess initial level	SS initial level	Units	Ref.
Buffers-Ca^{2+}	0.0	1.7	μM		MST1/2	1	0.974	μM	A
CaM	6	5.965	μM	(Khalilimeybodi et al., 2018)	MST1/2-p	0.0	0.026	μM	
CaM-Ca^{4+}	0.0	0.035	μM		LATS1/2	1	0.877	μM	A
		Kinases Module			LATS1/2-p	0.0	0.123	μM	
AKT	0.04	0.032	μM	(Legewie et al., 2008)	YAPTAZc	0.0	0.662	μM	
AKT-p	0.0	0.008	μM		YAPTAZc-p	0.0	0.152	μM	
CaMKII	20	19.998	μM	(Rangamani et al., 2016)	YAPTAZn	1	0.781	μM	(Scott et al., 2021)
CaMKII-p	0.0	0.002	μM		Myo	5	3.454	μM	(Scott et al., 2021)
JNK	1	0.988	μM	A	Myo*	0.0	1.546	μM	
JNK-p	0.0	0.012	μM		LaminA	0.0	1185.57	$\frac{molecules}{\mu m^2}$	
Pyk2	1	0.985	μM	A	LaminA-p	3500	2314.43	$\frac{molecules}{\mu m^2}$	(Scott et al., 2021)
Pyk2-p	0.0	0.015	μM		NPC	6.5	6.455	$\frac{molecules}{\mu m^2}$	(Scott et al., 2021)
aPKC	0.1	0.1	μM	A	NPC*	0.0	0.045	$\frac{molecules}{\mu m^2}$	
cPKC	0.57	0.522	μM	(Gordge et al., 1996)			**Other Mediators**		
cPKC- Ca^{2+}	0.0	0.031	μM		PP2Ac	1	0.96	μM	A
cPKC-Ca^{2+}-DAG	0.0	0.0	μM		PP2Ac*	0.0	0.04	μM	
cPKC-Ca^{2+}-DAG*	0.0	0.017	μM		TGS	1	0.8	μM	A
nPKC	0.33	0.33	μM	(Gordge et al., 1996)	TGS-m	0.0	0.2	μM	
nPKC-DAG	0.0	0.0	μM						

A: Assumed

Table 2

List of reactions and parameters in the GPCR and IP_3-Ca^{2+} modules

No.	Reaction	Reaction Rate	Par.	Value	Units
		GPCR Module			
R1	Ligand + GR ↔ L-GR	$R_1 = Kf_{r1}[Ligand][GR] - Kr_{r1}[L-GR]$	Kf_{r1} Kr_{r1}	5.0 $1.5Kf_{r1}\times10^{-3}$	$s^{-1}.\mu M^{-}$ s^{-1}
R2	L-GR + GqGDP ↔ L-GR-GqGDP	$R_2 = Kf_{r2}[L-GR][GqGDP] - Kr_{r2}[L-GR-GqGDP]$	Kf_{r2} Kr_{r2}	1.0 1.0×10^{-3}	$\mu m^2.s^{-1}.mole$ s^{-1}
R3	GqGDP + GR ↔ GR-GqGDP	$R_3 = Kf_{r3}[GqGDP][GR] - Kr_{r3}[GR-GqGDP]$	Kf_{r3} Kr_{r3}	2.75×10^{-4} 7.535	$\mu m^2.s^{-1}.mole$ s^{-1}
R4	Ligand + GR-GqGDP ↔ L-GR-GqGDP	$R_4 = Kf_{r4}[Ligand][GR-GqGDP] - Kr_{r4}[L-GR-GqGDP]$	Kf_{r4} Kr_{r4}	6.02×10^{-1} 9.03×10^{-4}	$s^{-1}.\mu M^{-}$ s^{-1}
R5	L-GR-GqGDP ↔ L-GR + GqGTP	$R_5 = Kf_{r5}[L-GR-GqGDP] - Kr_{r5}[L-GR][GqGTP]$	Kf_{r5} Kr_{r5}	2.22×10^{1} 0.0	s^{-1} $\mu m^2.s^{-1}.mole$
R6	L-GR-GqGDP ↔ L-GR-GqGDP-P	$R_6 = Kf_{r6}[L-GR-GqGDP] - Kr_{r6}[L-GR-GqGDP-p]$	Kf_{r6} Kr_{r6}	6.22×10^{-2} 0	s^{-1} s^{-1}
R6*	L-GR-GqGDP-p → GR + GqGDP + Ligand	$R_{6*} = Kf_{r6*}[L-GR-GqGDP-p]$	Kf_{r6*}	1.0	s^{-1}
R7	GqGTP ↔ GqGDP	$R_7 = Kf_{r7}[GqGTP] - Kr_{r7}[GqGDP]$	Kf_{r7} Kr_{r7}	1.5×10^{-1} 0	s^{-1} s^{-1}
		IP_3-Ca^{2+} Module			
R8	GqGTP + PLCβ ↔ GqGTP-PLCβ	$R_8 = Kf_{r8}[GqGTP][PLC\beta] - Kr_{r8}[GqGTP-PLC\beta]$	Kf_{r8} Kr_{r8}	4.2×10^{-2} 1.0	$\mu m^2.s^{-1}.mole$ s^{-1}
R9	Ca^{2+} + PLCβ ↔ Ca^{2+}-PLCβ	$R_9 = Kf_{r9}[Ca^{2+}][PLC\beta] - Kr_{r9}[Ca^{2+}-PLC\beta]$	Kf_{r9} Kr_{r9}	1.67×10^{-2} 1.67×10^{-2}	$s^{-1}.\mu M^{-}$ s^{-1}
R10	GqGTP + Ca^{2+}-PLCβ ↔ GqGTP-Ca^{2+}-PLCβ	$R_{10} = Kf_{r10}[GqGTP][Ca^{2+}-PLC\beta] - Kr_{r10}[GqGTP-Ca^{2+}-PLC\beta]$	Kf_{r10} Kr_{r10}	4.2×10^{-2} 1.0	$\mu m^2.s^{-1}.mole$ s^{-1}
R11	Ca^{2+} + GqGTP-PLCβ ↔	$R_{11} = Kf_{r11}[Ca^{2+}][GqGTP-PLC\beta] - Kr_{r11}[GqGTP-Ca^{2+}-PLC\beta]$	Kf_{r11} Kr_{r11}	3.34×10^{-2} 3.34×10^{-3}	$s^{-1}.\mu M^{-}$ s^{-1}

No.	Reaction	Reaction Rate	Par.	Value	Units
	GqGTP-Ca^{2+}-PLCβ				
R12	GqGTP-Ca^{2+}-PLCβ ↔ GqGDP + Ca^{2+}-PLCβ	$R_{12} = Kf_{r12}[GqGTP - Ca^{2+} - PLC\beta] - Kr_{r12}[GqGDP][Ca^{2+} - PLC\beta]$	Kf_{r12} Kr_{r12}	6.0 0	s^{-1} $\mu m^2 . s^2 . molec$
R13	GqGTP-PLCβ ↔ GqGDP + PLCβ	$R_{13} = Kf_{r13}[GqGTP - PLC\beta] - Kr_{r13}[GqGDP][PLC\beta]$	Kf_{r13} Kr_{r13}	6.0 0	s^{-1} $\mu m^2 . s^2 . molec$
R14	PIP2 → IP3 + DAG (E = *Ca^{2+}-PLCβ*)	$R_{14} = \frac{KIP3_{r14}[Ca^{2+} - PLC\beta][PIP2]}{Km_{r14} + [PIP2]}$	$KIP3_{r14}$ Km_{r14}	7.778×10^{-1} 2.176×10^{4}	s^{-1} $\mu m^2 . molecu$
R15	PIP2 → IP3 + DAG (E = *GqGTP-Ca^{2+}-PLCβ*)	$R_{15} = \frac{KIP3_{r15}[GqGTP - Ca^{2+} - PLC\beta][PIP2]}{Km_{r14} + [PIP2]}$	$KIP3_{r15}$ Km_{r15}	9.755 5.494×10^{3}	s^{-1} $\mu m^2 . molecu$
R16	IP3 → ∅	$R_{16} = Kf_{r16}[IP_3]$	Kf_{r16}	3.66×10^{-2}	s^{-1}
R17	DAG → ∅	$R_{17} = Kf_{r17}[DAG]$	Kf_{r17}	5.5×10^{-3}	s^{-1}
R18	→ PA (E = *Ligand*)	$R_{18} = Kf_{r18}[Ligand]$	Kf_{r18}	4.6	$\mu m^2 . s^{-1} . molecul$
R19	PA ↔ DAG	$R_{19} = Kf_{r19}[PA] - Kr_{r19}[DAG]$	Kf_{r19} Kr_{r19}	3.503×10^{2} 1.0×10^{4}	s^{-1} $\mu m^2 . s^{-1} . molecul$
R20	Ca^{2+} + Buffer ↔ Ca^{2+}-Buffer	$R_{20} = Kf_{r20}[Ca^{2+}][Buffer] - Kf_{r20}Kd_{Buff}[DAG]$	Kf_{r20} Kd_{Buff}	5.0×10^{2} 1.0×10^{1}	$s^{-1} . \mu M^{-}$ μM
R21	CaM + 4Ca^{2+} ↔ CaM-Ca^{2+}	$R_{21} = Kf_{r21}[CaM][Ca^{2+}]^4 - Kr_{r21}[CaM - Ca^{2+}]$	Kf_{r21} Kr_{r21}	1.0×10^{3} 1.0	$s^{-1} . \mu M^{-}$ s^{-1}
J_{IP3R}	Ca^{2+} (ER) → Ca^{2+}	$IP3R_{flux} = ([Ca_{ER}^{2+}] - [Ca^{2+}])v_1 \left(\frac{[Ca^{2+}][IP_3]d2}{([Ca^{2+}][IP_3] + [IP_3]d_2 + d_1d_2 + [Ca^{2+}]d_3)([Ca^{2+}] + d_4)}\right)^3$	v_1 d_1 d_2 d_3 d_4	10.0 1.3×10^{-1} 5.0×10^{-1} 9.4×10^{-3} 8.234×10^{-2}	$\mu m . s^{-1}$ μM μM μM μM
J_{ERleak}	Ca^{2+} (ER) → Ca^{2+}	$ERleak_{flux} = Kf_{ERleak}([Ca_{ER}^{2+}] - [Ca^{2+}])$	Kf_{ERleak}	2.1×10^{-3}	$\mu m . s^{-1}$
J_{SERCA}	Ca^{2+} → Ca^{2+} (ER)	$SERCA_{flux} = \frac{H([TGS] - TGS0)Vmax_s[Ca^{2+}]^{n_s}}{[Ca^{2+}]^{n_s} + Km_s^{n_s}}$	$Vmax_s$ n_s Km_s $TGS0$	1.9 1.0 5.0×10^{-1} 4.0×10^{-1}	$\mu m . s^{-1}$ 1 μM μM
J_{PMCA}	Ca^{2+} → Ca^{2+} (ECM)	$PMCA_{flux} = Y\frac{Vmax_p[Ca^{2+}]^{n_p}}{[Ca^{2+}]^{n_p} + Km_p^{n_p}}$	$Vmax_p$ n_p Km_p Y	2.5878 2.0 2.0×10^{-1} 6.0×10^{-1}	$\mu m . \mu M . s$ 1

No.	Reaction	Reaction Rate	Par.	Value	Units
					μM
					μM
J_{SOCE}	Ca^{2+} (ECM) $\rightarrow Ca^{2+}$	$SOCE_{flux} = Ymax_{SO}(1.0 - \frac{1.0}{1 + (\frac{Km_{so}}{[Ca_{ER}^{2+}]})^{n_{so}}})([Ca_{EX}^{2+}] - [Ca^{2+}])$	$Ymax_{SO}$	2.13×10^{-4}	$\mu m \,.\, s^{-1}$
			n_{so}	4.2	1
			Km_{so}	2.126×10^{1}	μM
J_{TRP}	Ca^{2+} (ECM) $\rightarrow Ca^{2+}$	$TRP_{flux} = \frac{Kf_{TRP} \,.\, Emol}{C_{TRP} + Emol}([Ca_{EX}^{2+}] - [Ca^{2+}])$	Kf_{TRP}	1.0×10^{-4}	$\mu m \,.\, s^{-1}$
			C_{TRP}	3.0	kPa
			$Emol$	$ECM_{Stiffness}$	kPa
J_{PMleak}	Ca^{2+} (ECM) $\rightarrow Ca^{2+}$	$PMleak_{flux} = Kf_{PM}([Ca_{EX}^{2+}] - [Ca^{2+}]) - K_{mit}H([TGSA] - TGS1)$	Kf_{PM}	3.31×10^{-5}	$\mu m \,.\, s^{-1}$
			K_{mit}	5.3×10^{-1}	$\mu m \,.\, s^{-1}$
			$TGS1$	4.1×10^{-1}	μM

E: Estimated

Table 3

List of reactions and parameters in the Kinases, RhoA, and F-actin modules

No.	Reaction	Reaction Rate
		Kinases Module
R22	AKT → AKT-p	$R_{22} = (Kf1_{r22}[CaMKII - p] - Kf2_{r22}[FAK - p])[\mathrm{AKT}]$
R23	AKT-p → AKT	$R_{23} = \frac{Kcat_{r23}[PP2Ac^*][AKT - p]}{Km_{r23} + [AKT - p]}$
R24	CaMKII → CaMKII-p	$R_{24} = \frac{Kcat1_{r24}([CaM - Ca^{2+}])^4[CaMKII]}{(Km1_{r24})^4 + ([CaM - Ca^{2+}])^4} + \frac{Kcat2_{r24}[CaMII - p][CaMKII]}{Km2_{r24} + [CaMKII]}$
R25	CaMKII-p → CaMKII	$R_{25} = \frac{Kcat_{r25}PP1[CaMKII - p]}{Km_{r25} + [CaMKII - p]}$
R26	JNK → JNK-p	$R_{26} = (Kf_{r26}[Ca^{2+}])[\mathrm{JNK}]$
R27	JNK-p → JNK	$R_{27} = \frac{Kcat_{r27}[PP2Ac^*][CaMKII - p]}{Km_{r27} + [CaMKII - p]}$
R28	Pyk2 ↔ Pyk2-p	$R_{28} = Kf_{r28}[CaMKII - p][Pyk2] - Kr_{r28}[Pyk2 - p]$
R29	nPKC + DAG ↔ nPKC-DAG	$R_{29} = Kf_{r29}[nPKC][DAG] - Kr_{r29}[nPKC - DAG]$
R30	cPKC + Ca^{2+} ↔ cPKC-Ca^{2+}	$R_{30} = Kf_{r30}[cPKC][Ca^{2+}] - Kr_{r30}[cPKC - Ca^{2+}]$
R31	cPKC-Ca^{2+} + DAG ↔ cPKC-Ca^{2+}-DAG	$R_{31} = Kf_{r31}[cPKC - Ca^{2+}][DAG] - Kr_{r31}[cPKC - Ca^{2+} - DAG]$
R32	cPKC-Ca^{2+}-DAG ↔ cPKC-Ca^{2+}-DAG*	$R_{32} = Kf_{r32}[F - actin][cPKC - Ca^{2+} - DAG] - Kr_{r32}[cPKC - Ca^{2+} - DAG^*]$
		RhoA Module
R33	FAK → FAK-p	$R_{33} = Kf_{r33}[FAK]$
R34	FAK → FAK-p	$R_{34} = \frac{Kcat_{r34}Emol[FAK]}{C + Emol}$
R35	FAK-p → FAK	$R_{35} = Kf_{r35}[FAK - p]$

No.	Reaction	Reaction Rate
R36	RhoAGDP → RhoAGTPMem.	$R_{36} = (Kf1_{r36}(1 + \gamma[FAK]^{n_f}) + Kf2_{r36}[Pyk2 - p])\,[RhoAGDP]$
R37	RhoAGTPMem. → RhoAGDP	$R_{37} = Kf_{r37}[RhoAGTPMem]$
R38	ROCK → ROCK*	$R_{38} = Kf_{r38}[RhoAGTPMem.][ROCK]$
R39	ROCK* → ROCK	$R_{39} = Kf_{r39}[ROCK^*]$
R40	mDia → mDia*	$R_{40} = Kf_{r40}[RhoAGTPMem.][mDia]$
R41	mDia* → mDia	$R_{41} = Kf_{r41}[mDia^*]$
		F-actin Module
R42	G-actin ↔ F-actin	$R_{42} = (Kf1_{r42}\left(1.0 + 0.5\alpha\left(1 + \tanh\left(20.0([mDia^*] - mDiaT)\right)[mDia^*]\right) + Kf2_{r42}[APR2\,/\,3^*] + Kf3_{r42}[Ca^{2+}]\right)[G_{actin}]$ $(Kr1_{r42} + Kr2_{r42}[Cofilin - p])[F_{actin}]$
R43	LIMK ↔ LIMK*	$R_{43} = (Kf1_{r43}\left(1.0 + 0.5\tau\left(1 + \tanh\left(20.0([ROCK^*] - ROCKT)\right)[ROCK^*]\right) + Kf2_{r43}[CaMKII - p]\right)[LIMK] - Kr_{r3}[LIM$
R44	Cofilin-p ↔ Cofilin	$R_{44} = Kf_{r44}[Cofilin - p] - \frac{Kcat_{r44}[LIMK^*][Cofilin]}{Km_{r44} + [Cofilin]}$
R45	Merlin ↔ Merlin*	$R_{45} = Kf_{r45}[Ca^{2+}][F_{actin}][Merlin] - Kr_{r45}[Merlin^*]$
R46	Arp23 ↔ Arp23*	$R_{46} = Kf_{r46}[CaMKII - p][Apr23] - Kr_{r46}[Apr23^*]$

E: Estimated

Table 4

List of reactions and parameters in the Hippo-YAP/TAZ module

No.	Reaction	Reaction Rate	Par.	Value	Units
		Hippo-YAP/TAZ Module			
R47	MST12 → MST12-p	$R_{47} = \frac{Kcat_{r47}\, H([cPKC - Ca^{2+} - DAG^*] - cPKCT)[MST12]}{(Km_{r47} + [AKT - p]) + [MST12]}$	$Kcat_{r47}$ $cPKCT$ Km_{r47}	1.0×10^{1} 1.3×10^{-2} 1.0×10^{-1}	
R48	MST12-p → MST12	$R_{48} = \frac{Kcat_{r48}[PP2Ac^*][MST12 - p]}{Km_{r48} + [MST12 - p]}$	$Kcat_{r48}$ Km_{r48}	4.0×10^{1} 1.0	
R49	LATS12 → LATS12-p	$R_{49} = \frac{\left(\frac{Kcat1_{r49}}{[aPKC]}[MST12 - p] + Kcat2_{r49}[Merlin^*] + Kcat3_{r49}[nPKC - DAG]\right)[LATS12]}{Km1_{r49}[JNK - p] + Km2_{r49}[cPKC - Ca^{2+} - DAG^*] + [LATS12]}$	$Kcat1_{r49}$ $Kcat2_{r49}$ $Kcat3_{r49}$ $Km1_{r49}$ $Km2_{r49}$	4.0×10^{-1} 1.0 1.0×10^{2} 1.0	
R50	LATS12-p → LATS12	$R_{50} = \frac{Kcat_{r50}[PP2Ac^*][LATS12 - p]}{Km_{r50} + [LATS12 - p]}$	$Kcat_{r50}$ Km_{r50}	$Kcat_{r48}$ Km_{r48}	
R51	Myo ↔ Myo*	$R51 = Kf_{r51}\left(1 + 0.5eps\left(1 + \tanh\left(20([ROCK^*] - ROCKT)\right)\right)[ROCK^*]\right)[Myo] - Kr_{r51}[Myo^*]$	Kf_{r51} eps $ROCKT$ Kr_{r51}	3.0×10^{-2} 3.6×10^{1} 3.0×10^{-1} 6.7×10^{-2}	
R52	LaminA-p ↔ LaminA	$R52 = \frac{Kf_{r52}E_{cyt}}{Km_{r52} + E_{cyt}}[LaminA - p] - Kr_{r52}[LaminA]$ $E_{cyt} = K_E[F_{actin}]^{ne}$	Kf_{r52} $Km2_{r52}$ K_E ne Kr_{r52}	6.0×10^{-2} 1.0×10^{2} 3.8×10^{-5} 2.1 1.0×10^{-3}	
R53	NPC ↔ NPC*	$R53 = Kf_{r53}[Myo^*][F_{actin}][LaminA][NPC] - Kr_{r51}[NPC^*]$	Kf_{r51} Kr_{r51}	2.8×10^{-7} 8.7	μm^2
R54	YAPTAZc ↔ YAPTAZc-p	$R54 = \frac{Kcat_{r54}[LATS12 - p][YAPTAZc]}{Km_{r54} + [YAPTAZc]}$	$Kcat_{r54}$ Km_{r54}	1.0×10^{2} 1.0	
R55	YAPTAZc-p ↔ YAPTAZc	$R55 = Kf_{r55}[Myo^*][F_{actin}][YAPTAZc - p] - Kr_{r55}[YAPTAZc]$	Kf_{r55} Kr_{r55}	2.0×10^{-1} 1.0	
R56	YAPTAZc ↔ YAPTAZn	$R56 = (Kf1_{r56}[NPC^*] + Kf2_{r56})[YAPTAZc] - Kr_{r56}[YAPTAZn]$	$Kf1_{r56}$ $Kf2_{r56}$ Kr_{r56}	4.0 1.0 1.0	μm^{-2} μm^{-2}
		Other Mediators			
R57	PP2Ac ↔ PP2Ac*	$R57 = (Kf1_{r57}[Ligand] + Kf2_{r57}[TG] + Kf3_{r57})[PP2AC] - Kr_{r57}[PP2Ac^*]$	$Kf1_{r57}$ $Kf2_{r57}$ $Kf3_{r57}$ Kr_{r57}	4.7×10^{-5} 1.128×10^{-6} 3.882×10^{-6} 9.44×10^{-5}	

Health Research Alliance Author Manuscript

No.	Reaction	Reaction Rate	Par.	Value	Units
R58	TGS ↔ TGS-m	$R58 = (Kf1_{r58}[TG] + TGbasal)[TGS] - 4.0 * TGbasal[PP2Ac^*]$	$Kf1_{r58}$ $TGbasal$	1.35×10^{-3} 2.7×10^{-4}	

E: Estimated

Table 5

Prediction of Ca^{2+}-YAP/TAZ relationship in different experimental settings

No.	Study	Perturbation	Ca^{2+} (Exp.)	Ca^{2+} (Model)	YAP/TAZ activity (Exp.)	YAP/TAZ activity (Model)
1	D'Amore et al. (2020)	TPC2-KO (Orai1-i & cPKC-i)	Not reported	↓	↑	↑
2	Dang et al. (2019)	SPCA2-overexpression	↑	↑	↓	↓
3	Deng et al. (2020)	Thermal cycles	↑	↑	↓	↓
4	Franklin et al. (2020)	Thapsigargin	↑	↑	↓ (YAP/TAZ N/C) ↑ (Localization reset)	↓(YAP/TAZ N/C) ↑(Localization reset)
5	Pathak et al. (2014)	Piezo1	↑	↑	↑	↑
6	Wang et al. (2020)	Ionomycin	↑	↑	↑	↑